Structural basis of meiotic chromosome synapsis through SYCP1 self-assembly

Authors

James M. Dunce[1], Orla M. Dunne[1], Matthew Ratcliff[1,4], Claudia Millán[2], Suzanne Madgwick[1], Isabel Usón[2,3], Owen R. Davies[1]

Affiliations

[1]Institute for Cell and Molecular Biosciences, Newcastle University, Newcastle upon Tyne, UK.

[2]Crystallographic Methods, Institute of Molecular Biology of Barcelona (IBMB-CSIC), Barcelona, Spain.

[3]ICREA, Institució Catalana de Recerca i Estudis Avançats, Barcelona, Spain.

[4]Present address: Department of Biochemistry, University of Cambridge, UK.

Author for Correspondence

Owen R. Davies: owen.davies@newcastle.ac.uk

Abstract

Meiotic chromosomes adopt unique structures in which linear arrays of chromatin loops are bound together in homologous chromosome pairs by a supramolecular protein assembly, the synaptonemal complex. This three-dimensional scaffold provides the essential structural framework for genetic exchange by crossing over and subsequent homologue segregation. The core architecture of the synaptonemal complex is provided by SYCP1. Here, we report the structure and self-assembly mechanism of human SYCP1 through X-ray crystallographic and biophysical studies. SYCP1 has an obligate tetrameric structure in which an N-terminal four-helical bundle bifurcates into two elongated C-terminal dimeric coiled-coils. This building-block assembles into a zipper-like lattice through two self-assembly sites. N-terminal sites undergo cooperative head-to-head assembly in the midline, whilst C-terminal sites interact back-to-back on the chromosome axis. Our work reveals the underlying molecular structure of the synaptonemal complex in which SYCP1 self-assembly generates a supramolecular lattice that mediates meiotic chromosome synapsis.

Keywords

Meiosis, chromosome structure, double-strand break, chiasmata, synaptonemal complex, SYCP1, self-assembly

Introduction

The reduction in chromosome number during meiosis requires a unique programme of intricate molecular processes including the synapsis of homologous chromosome pairs, their exchange of genetic material by crossing over, and ultimately their segregation into haploid cells. At the centre of these processes is a supramolecular protein assembly, the synaptonemal complex (SC). The SC binds together homologous chromosome pairs, structured as linear arrays of chromatin loops, in a single continuous synapsis along their entire length[1,2]. SC assembly occurs in a spatiotemporal manner, dependent on the prior establishment of inter-homologue recombination intermediates through double-strand break induction, which act as guides to ensure the synapsis of perfectly aligned homologues[3,4]. The three-dimensional structure of the SC provides the essential architectural framework for the resolution of recombination intermediates, which includes the generation of one genetic crossover per chromosome arm[5,6]. Crossovers are essential for correct segregation of homologues at anaphase I, and additionally contribute to genetic diversity. The defective assembly of the SC is associated with human infertility, miscarriage and aneuploidy[7,8]. However, despite its discovery more than half a century ago, the molecular structure and function of the SC have remained unknown.

Electron micrographs of the SC reveal a characteristic tripartite structure that is conserved across eukaryotes[9]. This consists of two lateral elements, each coating a chromosome axis, separated by a 100 nm central region that contains a midline 20-40 nm wide central element (Fig. 1a). The central and lateral elements are connected together by a network of angled transverse filaments, which in hamster have a diameter of approximately 16 Å and are spaced at a density of 50-80 per 1 µm of chromosome axis[10]. In addition to its 100 nm width, the SC central region has a depth of up to 100 nm, so is a truly three-dimensional protein assembly[11,12].

In mammals, SC transverse filaments are formed by SYCP1[13]. This 976 amino acid protein contains a central α-helical core flanked by unstructured N- and C-terminal tails (Fig. 1b). SYCP1 N- and C-termini are localised within SC central and lateral elements respectively, and so is bioriented with juxtaposed SYCP1 molecules providing a 150 nm separation between opposing C-termini in mice[12,14,15] (Fig. 1a). The SC contains at least two layers of SYCP1 molecules; N-termini are detected in two vertically separated chains within the central element, whereas C-termini are present in a single chain within the lateral element[12,16]. SC lateral elements also contain SYCP2 and SYCP3[17,18], the latter contributing to chromosome compaction through stabilisation of chromatin loop structures[19-21]. The SC central element contains initiation factors SYCE3, SYCE1 and SIX6OS1 that stabilise initial tripartite structures[22-25], and elongation complex SYCE2-TEX12 that stabilises the long-range extension of the tripartite structure[26-29].

SYCP1 disruption leads to a complete failure of synapsis; recombination intermediates are formed but fail to resolve, crossovers fail to form, cells undergo meiotic arrest and there is a resultant complete infertility[5]. Whilst SC central and lateral element components are essential for the structure and function of the mature SC, SYCP1 is recruited to meiotic chromosomes in the absence of other SC central and lateral element components, albeit at reduced levels, and is essential for the recruitment of all SC central element proteins[5,17,18,22,23,25-28]. Furthermore, SYCP1 in isolation has an intrinsic capacity for self-assembly into rudimentary SC-like structures[30]. Thus, SYCP1 self-assembly seemingly provides the underlying architectural framework of the SC.

Here, we report the structure and self-assembly mechanism of SYCP1. The obligate unassembled structure of SYCP1 is an N-terminal tetramer that bifurcates into two elongated C-terminal dimeric coiled-coils. This building-block self-assembles into a supramolecular lattice that defines the SC structure through sites within its N- and C-termini. Whilst N-terminal sites undergo cooperative head-to-head assembly, C-terminal sites interact back-to-back in a protonation-dependent manner

that relies upon chromosomal recruitment by unstructured C-terminal tails. Together, our data lead to a complete molecular model for the structure of SYCP1 in which recursive self-assembly at N- and C-terminal sites leads to the formation of a continuous and cooperative supramolecular lattice. Through this, we reveal the underlying structure of the synaptonemal complex and the molecular basis of meiotic chromosome synapsis by SYCP1.

Results

The obligate structure of SYCP1

Human SYCP1 contains a large α-helical core (αCore) of amino acids 101-783, flanked by unstructured N- and C-terminal tails (Fig. 1b and Supplementary Fig. 1a). Size-exclusion chromatography multi-angle light scattering (SEC-MALS) analysis of purified recombinant SYCP1 αCore revealed heterogeneous 1-12 MDa species (Fig. 1c and Supplementary Fig. 1b), indicating an intrinsic capacity to self-assemble *in vitro*. Self-assembly of large molecular weight species is completely abrogated by deletion of the first 11 amino acids at its N-terminal tip (αN-tip), with αCore-ΔNtip (residues 112-783) forming a stable tetramer (Fig. 1c). Circular dichroism (CD) spectroscopy confirms that αCore-ΔNtip is almost entirely α-helical (Supplementary Fig. 2a,b). Size exclusion chromatography small-angle X-ray scattering (SEC-SAXS) analysis reveals scattering profiles and real space pair-distance distribution functions (P(r) distributions) corresponding to an elongated molecule of 900 Å length (Fig. 1d and Supplementary Fig. 2c). This matches its theoretical α-helical coiled-coil length and is sufficient to span just over half of the inter-chromosomal distance, in keeping with SYCP1 biorientation within the SC. We conclude that αCore-ΔNtip is an extended α-helical coiled-coil tetramer that represents the obligate structure of SYCP1, and self-assembly of this minimum building-block into higher molecular weight species is dependent on the N-terminal tip of SYCP1 αCore.

The obligate αCore-ΔNtip is composed of two distinct structural units, an N-terminal tetramer (residues 206-362) and C-terminal dimer (residues 358-783) (Fig. 1c). These boundaries were identified through exhaustive screening to define clearly demarcated structural regions of maximal stability; nevertheless, oligomer states and structures of these and other constructs described herein are robust across a range of sequence boundaries (Supplementary Fig. 1a and Supplementary Table 1). The αN-tetramer and αC-dimer are almost entirely α-helical (Supplementary Fig. 2a,b); SEC-SAXS analysis reveals elongated structures of respective lengths 260 Å and 645 Å (Fig. 1d and

Supplementary Fig. 2c-e), matching their theoretical coiled-coil lengths. The cross-sectional radius of gyration (Rc) was determined as 10.3 Å and 8.9 Å for αN-tetramer and αC-dimer (Supplementary Fig. 2f), corresponding to the known dimensions of four-helical and dimeric coiled-coils respectively. The Rc of αC-dimer (8.9 Å) indicates a diameter of 17.8 Å that closely matches the measured 16 Å diameter of transverse filaments in the hamster SC[10], suggesting that αC-dimers constitute the individual structures visualised spanning between SC central and lateral elements.

We determined the orientation of helices within αCore-ΔNtip, αN-tetramer and αC-dimer through SEC-SAXS P(r) analysis of N-terminal MBP fusion proteins, exploiting the strong scattering of globular proteins in comparison to coiled-coils to identify the relative positions of globular tags. In all cases, P(r) distributions demonstrate strong inter-MBP peaks at short distances, compatible with their parallel orientation, but lack inter-MBP peaks at long distances that would occur in anti-parallel structures (Fig. 1e and Supplementary Fig. 2d-h). Similarly, an N-terminal GST fusion of αN-tetramer shows only short distance inter-GST peaks (Supplementary Fig.2 j-n). Finally, the αN-tetramer and αC-dimer structures are compatible with their N-terminal fusion to a constitutive tetramer (RecE) and dimer (GST) respectively (Fig. 1f and Supplementary Fig. 2i-n), confirming their parallel orientation. Thus, αCore-ΔNtip, αN-tetramer and αC-dimer are parallel coiled-coils, in keeping with the biorientation of SYCP1 molecules within the SC. We conclude that the obligate structure of SYCP1, which provides the minimal building block for self-assembly, is an N-terminal four-helical bundle that bifurcates into C-terminal dimeric coiled-coils of sufficient length to span between SC central and lateral elements (Fig. 1g).

SYCP1 N-terminal self-assembly

The αN-tip (residues 101-111) is essential for self-assembly of αCore into large molecular weight species *in vitro* and is part of a short αN-end region (residues 101-206), immediately preceding the αN-tetramer, that is the most highly conserved portion of SYCP1 (Fig. 1b). The X-ray crystal

158 structures of two αN-end constructs (residues 101-206 and 101-175) reveal tetrameric assemblies in
159 which two parallel dimeric coiled-coils interact head-to-head (Fig. 2a,b, Supplementary Fig. 3 and
160 Table 1). The head-to-head interface is mediated entirely by the αN-tip (Fig. 2a,b), suggesting that
161 this 'dimer of dimers' structure may be responsible for SYCP1 N-terminal self-assembly into higher
162 order structures.
163
164 The two αN-end crystal structures demonstrate a common fold in which parallel dimeric coiled-coils
165 splay apart through a wedge formed of W119 and I116 to allow the αN-tips of opposing molecules to
166 interact head-to-head (Figs. 2a,b and 3a,d). The head-to-head interface shows distinct but highly
167 related conformations in the two structures, indicating conformational plasticity. The open
168 conformation of αN-end is asymmetrical and crescent-shaped, formed of midline and lateral anti-
169 parallel coiled-coil interactions (Figs. 2a and 3a-c,g). The closed conformation of truncated αN-end is
170 a symmetrical four-helical bundle, consisting of a hydrophobic core and analogous midline and
171 lateral helical interfaces (Figs. 2b and 3d-f,h). The two conformations are formed of identical amino
172 acids undergoing largely similar coiled-coil and aromatic stacking interactions (Fig. 3b-c,e-h), and
173 likely exist in equilibrium, undergoing conformational change through a rotamer flip of central Y106
174 residues (Fig. 3g,h and Supplementary Fig. 3e). This structural plasticity may be important in
175 enforcing synapsis whilst accommodating large-scale twisting and bending of synapsed meiotic
176 chromosomes, with the open conformation permitting wider angulation between opposing SYCP1
177 molecules than the more rigid closed conformation.
178
179 SYCP1 αCore self-assembly is recapitulated by construct αN (residues 101-362) that includes both
180 αN-end and αN-tetramer (Fig. 4a and Supplementary Fig. 4a,b). Its self-assembly into large
181 molecular weight species is blocked by removal of either sequence, and is retained in the presence
182 of the unstructured N-terminal tail (Fig. 4a,b and Supplementary Fig. 4c-e). Thus, the presence of
183 αN-end and αN-tetramer is necessary and sufficient for SYCP1 N-terminal self-assembly *in vitro*.

Mutation of head-to-head interacting residues V105 and L109 to glutamate completely abrogates αN self-assembly into large molecular weight species, leaving a stable obligate tetramer (Fig. 4a). Thus, the αN-end head-to-head interaction is likely responsible for SYCP1 N-terminal self-assembly. We propose that the αN-tetramer provides a structural scaffold from which two αN-end dimers splay apart, with their αN-tips interacting head-to-head with opposing SYCP1 molecules. A staggered configuration provides a simple model for the cooperative assembly of a continuous lattice structure of potentially limitless length, which we propose defines the structural basis of midline SYCP1 N-terminal self-assembly (Fig. 4c).

Isolated αN-end is monomeric (Fig. 4b), indicating that individual head-to-head interactions are weak and only form when the αN-tetramer mediates lattice formation. This requirement for cooperativity favours the self-assembly of a single continuous lattice between appropriately aligned meiotic chromosomes rather than forming heavily branched unproductive cellular assemblies (Fig. 4d).

SYCP1 C-terminal self-assembly

A highly conserved sequence at the C-terminal end of SYCP αCore caps off the αC-dimer parallel coiled-coil (Fig. 1b). The X-ray crystal structure of αC-end (residues 676-770) reveals an anti-parallel tetramer in which two αC-end parallel dimers interact back-to-back in an intertwined α-helical assembly (Fig. 5, Supplementary Fig. 5 and Table 1). We suggest that this αC-end tetrameric assembly provides the structural basis for SYCP1 C-terminal self-assembly on the chromosome axis.

In solution, αC-end is dimeric at pH 8.0 and tetrameric at pH 5.5 (Fig. 6a and Supplementary Fig. 6a,b). SEC-SAXS reveals that both species have similar length, but the cross-sectional radius increases from 7.8 Å to 10.1 Å at pH 5.5, consistent with a transition from dimeric to four-helical coiled-coil (Fig. 6b and Supplementary Fig. 6c-e). SAXS *ab initio* envelopes of the pH 8.0 and pH 5.5

species match the dimensions of a dimeric coiled-coil and the αC-end tetramer structure respectively (Fig. 6c,d). SEC-SAXS P(r) distributions of MBP fusions of αC-end at pH 8.0 show inter-MBP peaks at short distances, compatible with their parallel orientation; peaks at long anti-parallel distances were observed only upon MBP fusion at both termini, and for MBP-αC-end upon tetrameric assembly at pH 5.5 (Fig. 6e and Supplementary Fig. 6f-j). Similarly, GST-αC-end forms a stable dimer at pH 8.0 (Supplementary Fig. 6h-k). Finally, a tethered dimer of two consecutive αC-end sequences joined by a flexible linker is dimeric at pH 8.0, with length 241 Å and cross-sectional radius 8.8 Å, consistent with it forming two consecutive dimeric coiled-coils (Figs. 6f,g and Supplementary Fig. 6c-e). It remains dimeric at pH 5.5, but becomes a compact molecule of length 156 Å and cross-sectional radius 10.7 Å, indicating the folding back of αC-end sequences into an anti-parallel tetramer (Figs. 6f,g and Supplementary Fig. 6c-e). We conclude that αC-end is a parallel dimeric coiled-coil that undergoes pH-induced back-to-back assembly into the anti-parallel tetramer observed in the crystal structure.

The αC-end crystal structure has a highly conserved central tetrameric interface in which H717 and Y721 residues (invariant throughout vertebrates) form a hydrophobic core and engage in hydrogen bonding networks with Q720 residues (Figs. 1b and 5a,b, Supplementary Figs. 1a and 5g). The position of H717 residues suggested that their protonation may mediate pH-induced assembly. We introduced mutation H717W Y721F, designed to stabilise the core whilst eliminating pH-sensitivity (Supplementary Fig. 5h), into an extended αC-end construct (residues 676-783) that accentuates the elution difference between dimer and tetramer (Supplementary Fig. 7). H717W Y721F is tetrameric at pH 8.0 (Fig. 6h and Supplementary Fig. 7j), suggesting that pH-induced assembly in wild type involves stabilisation of the core through H717 protonation. Accordingly, mutation H717E blocked pH-induced tetrameric assembly (Supplementary Fig. 7k).

The central interface leads to pinch points, where N-terminal parallel coiled-coil dimers are flanked by angulated C-terminal chains (Fig. 5a,c,d). The coiled-coil includes C703 heptad interactions that are disulphide and non-disulphide at the respective smoothly and sharply angulated ends of the molecule. An alternative αC-end crystal form contains symmetry-related pinch points with C703 partial disulphide bonds and smoothly angulated flanking chains (Supplementary Fig. 5). Whilst disulphide bond formation may be a crystallisation artefact, it may also provide an intriguing means for stabilising assembly *in vivo*; notably, the αN-end head-to-head assembly includes similar heptad interactions between pairs of C183 and C190 residues.

The ends of the tetrameric structure are formed of four-helical bundles, consisting of a hydrophobic core and anti-parallel coiled-coil interfaces (Fig. 5a,e-g). Hydrophobic core residues outline heptad repeats within N- and C-terminal chains, with the latter constituting a three-heptad leucine zipper (Fig. 5g). These residues likely also mediate parallel coiled-coil interactions in the dimeric conformation. Amino acids L679 and I688 mediate anti-parallel interactions but lie outwith the hydrophobic core heptads, so may be specific for the tetramer. The mutation L679A I688A eliminated tetramer assembly but retained dimer formation (Fig. 6h and Supplementary Fig. 7l). We conclude that heptad residues of the αC-end termini are bifunctional in mediating parallel dimeric and anti-parallel tetrameric interactions, with the conformational change triggered by structural alteration of the protonation-sensitive central interface.

In the cell, back-to-back assembly of αC-end may be triggered by its concentration on the chromosome axis, through local protonation induced by the high proton density in the close proximity of DNA[31] or by specific interactions with chromosome axis proteins. Thus, protonation-dependent conformational change of αC-end provides an elegant mechanism for triggering SYCP1 C-terminal self-assembly upon chromosomal recruitment.

DNA binding by SYCP1

The αC-end tetrameric structure contains a series of surface basic patches separated by ~30 Å (Fig. 7a), suggesting a direct interaction with the DNA backbone. Analysis by electrophoretic mobility shift assay (EMSA) revealed strong double-stranded DNA binding of tetrameric αC-end at pH 5.5, but not of the dimer at pH 8.0 (Fig. 7b). The presence of DNA-binding interfaces on both surfaces of the αC-end tetramer could mediate the formation of large protein-DNA assemblies, possibly accounting for the range of species observed. The αC-end tetrameric conformation is likely stabilised by interaction with DNA, and so SYCP1 C-terminal self-assembly and DNA-binding may be mutually reinforcing.

How is the SYCP1 C-terminus first recruited to chromosomes? The SYCP1 C-terminal tail contains basic patches that could be obligate DNA-binding sites. A C-terminal construct including both αC-end and Ctail (residues 640-976) interacts with DNA at neutral pH; DNA-binding is dependent on the Ctail and is diminished upon deletion of αC-end (Fig. 7c and Supplementary Fig. 8a-d). We observe slightly enhanced DNA-binding at neutral pH by SYCP1 constructs extended N-terminally to include the αC-dimer and αCore (residues 358-976 and 101-976) (Fig. 7c and Supplementary Fig. 8e-h). Electron microscopy reveals the formation of ~10 nm wide protein-DNA complexes by αC-end~Ctail, which develop a wider frayed appearance upon inclusion of the αC-dimer, consistent with transverse filaments emanating from a core protein-DNA structure (Fig. 7d). Finally, we tested DNA-binding of full length SYCP1 using refolded protein that demonstrates α-helical structure and higher order assembly consistent with our findings for αCore (Supplementary Fig. 9). Full length SYCP1 interacts with DNA at neutral pH, and the interaction is disrupted by deletion of the Ctail (Fig. 7e). Together, these data demonstrate that SYCP1 binds DNA through its Ctail and the interaction is enhanced by the αC-end and wider SYCP1 structure.

We propose that SYCP1 molecules are recruited to meiotic chromosomes through sites within Ctails, leading to their concentration on chromatin. The close proximity of DNA and/or interactions with

287 axis proteins then triggers protonation-induced assembly of αC-end into tetramers that bind DNA
288 and strengthen axis associations. The anti-parallel αC-end tetramers also mediate back-to-back
289 interactions between SYCP1 molecules, which given their known orientation within the SC, likely
290 result in looped U-shaped linkages between adjacent αC-dimer transverse filaments (Fig. 7f). Thus,
291 SYCP1 C-terminal self-assembly integrates DNA-binding and interactions between adjacent
292 transverse filaments to achieve SYCP1 coating of chromosome axes.
293

Discussion

We integrate our crystallographic and biophysical findings into a molecular model for meiotic chromosome synapsis by SYCP1. The SYCP1 core consists of an αN-tetramer that bifurcates into two αC-dimers (Fig. 8a). This tetrameric building-block self-assembles into a supramolecular lattice through its N- and C-terminal ends. In the midline, αN-end dimers splay from αN-tetramer scaffolds and interact head-to-head in a highly cooperative lattice. In the lateral element, αC-end dimers assemble back-to-back as discrete intertwined tetramers that tether together adjacent αC-dimer transverse filaments and reinforce chromosomal associations of C-terminal tails. Together, N- and C-terminal self-assembly collaborate to generate a cooperative zipper-like supramolecular lattice of SYCP1 molecules capable of mediating continuous synapsis between homologous chromosomes (Fig. 8b). During SC assembly, midline lattice formation and chromosomal recruitment likely occur concomitantly in one dynamic process of progressive chromosome synapsis. Whilst we cannot exclude additional roles for N- and C-terminal tails in SYCP1 assembly *in vivo*, these regions are largely unstructured and have no effect on oligomer states *in vitro*. Conserved amino acid sequences within C-terminal tails may mediate currently unidentified interactions with chromosome axis proteins, which act in concert with direct DNA-binding to achieve meiotic chromosome recruitment of SYCP1.

Our model for SYCP1 self-assembly is consistent with the dimensions of the native SC. The SYCP1 tetrameric core has a length of 900 Å, sufficient to span just over half of the inter-chromosomal distance. The αC-dimer has an 8.9 Å cross-sectional radius and 645 Å length, matching the dimensions of individual transverse filaments measured by electron microscopy in the hamster SC[10]. We propose that αC-dimers constitute the transverse filaments visualised spanning between central and lateral elements, with αN-tetramers buried within the central element. Importantly, anti-parallel tetramer formation by αC-end explains how parallel SYCP1 molecules interact back-to-back to achieve the well-established biorientation of SYCP1 N- and C-termini within the SC[12,14,15]. A recent

study reported that a region similar to αC-end is an anti-parallel dimer[32], incompatible with established localisation patterns. Examination of their structural data (pdb 4YTO) reveals the presence of an anti-parallel tetramer within the crystal lattice, indicating that the anti-parallel dimer of the asymmetric unit was incorrectly attributed as the biological molecule (Supplementary Figure 5i).

The three-dimensional SC assembly contains at least two layers of transverse filament proteins[11,12,16], which is compatible with the SYCP1 supramolecular assembly that we describe. We propose that two parallel head-to-head SYCP1 lattices are connected by vertically (or obliquely) orientated back-to-back assemblies within lateral elements (Supplementary Fig. 10a). This model is consistent with the observed vertical separation of SYCP1 N-termini by up to 100 nm, and the presence of single tracks of SYCP1 C-termini within lateral elements[12,16].

How is SYCP1 self-assembly directed to occur predominantly between aligned chromosomes? Whilst SYCP1 can form chromatin-free polycomplexes in meiotic tissue[33], assembly into SCs is heavily favoured. Two distinct mechanisms cooperate to favour timely SYCP1 self-assembly between aligned chromosomes. Firstly, αN-end head-to-head interactions are individually weak and thus the prior accumulation of juxtaposed SYCP1 molecules between aligned chromosomes may nucleate its cooperative supramolecular assembly. Secondly, αC-end self-assembly occurs through a protonation-induced conformational change triggered by the proton density in the immediate vicinity of DNA[31] and/or axis protein interactions, thereby coupling assembly to chromosomal recruitment.

The nascent synapsis generated by SYCP1 self-assembly is stabilised and matured into a full SC through assembly of central element proteins SYCE3, SYCE1, SIX6OS1 and SYCE2-TEX12[16,22,23,25-29]. Their recruitment is dependent on SYCP1 and is essential for the tripartite structure and meiotic

346 function of the SC[22,23,25-28]. Central element assembly likely occurs concomitantly with SYCP1 self-
347 assembly, rapidly converting the underpinning SYCP1 structural framework into a mature SC. Initial
348 SYCP1 assemblies recruit central element proteins to stabilise the nascent lattice, enabling its
349 growth, and providing a mutually reinforcing cycle that results in full synapsis (Fig. 8c). Central
350 element proteins may provide vertical and longitudinal supports between αN-tetramers that rigidify
351 SYCP1 hemi-lattices and orientate αN-end sites for long-range cooperative head-to-head assembly
352 (Fig. 8d and Supplementary Fig. 10b). They may further act as transverse bridges that connect hemi-
353 lattices across the midline to directly reinforce αN-end head-to-head interactions. Initiation factors
354 SYCE3, SYCE1 and SIX6OS1 may act as transverse bridges and vertical supports[22-25], whilst SYCE2-
355 TEX12 may provide longitudinal supports that enable SC elongation[26-29]. This results in a mature SC in
356 which an underlying SYCP1 lattice is structurally supported by the central element. The true
357 molecular roles of SC central element proteins will be revealed upon their structure elucidation, and
358 it will be intriguing to see whether they simply dock onto the SYCP1 lattice or induce structural
359 remodelling upon recruitment.
360
361 Whilst SYCP1 chromosome axis recruitment is retained upon disruption of SC lateral element
362 proteins, synapsis is discontinuous, indicating that chromosome axis structure facilitates the efficient
363 loading of SYCP1 necessary for continuous synapsis[17,18,20]. This may occur through positioning
364 chromatin loops to achieve a regular spacing of SYCP1 molecules that is compatible with long-range
365 lattice formation. SYCP1 loading may similarly be regulated by the underlying chromatin structure.
366 For example, if both surfaces of αC-end tetramers interact with DNA, they may sit between adjacent
367 nucleosomes and would by spaced apart by the 11 nm nucleosome diameter.
368
369 How is the SC supramolecular structure efficiently disassembled following its function in meiosis?
370 SYCP1 self-assembly is intrinsic to the protein sequence and hence independent of post-translational
371 modifications, but phosphorylation has been implicated in SC disassembly[34]. Whilst there are no

clear candidate sites within SYCP1 αN-end or αC-end, phosphorylation of the numerous predicted sites within the C-terminal tail could destabilise axis assembly. Similarly, central element protein phosphorylation could destabilise SYCP1 midline lattice assembly. The molecular features of αN-end and αC-end that achieve cooperative assembly may facilitate the continuous turnover of SYCP1 molecules within the SC. Whilst dynamic interchange will normally lead to continual renewal of the SYCP1 lattice, phosphorylation-induced destabilisation of self-assembly sites would shift the balance towards a net loss of molecules and ultimately disassembly.

SYCP1 fulfils the classic functions of coiled-coil proteins in acting as molecular spacers that scaffold supramolecular assemblies and separate functional units[35]. SYCP1 imposes a 100 nm synapsis between homologous chromosomes, raising the question of why it is necessary to impose an evolutionarily conserved separation between homologues? This distance may be optimal for the maintenance and resolution of meiotic recombination intermediates, and so an answer may lie in differences in recombination in the few meiotic organisms that lack an SC[1]. Interestingly, the SC central region and central element are approximately 10% narrower in female mice than in males[36]. This variation can be accommodated by the SYCP1 lattice that we propose through alteration in angulation of αN-end assemblies and αC-dimers (Supplementary Fig. 10c). Furthermore, midline angulation and SC central region width are determined by the frequency of αC-end binding to chromosomes; thus, midline variation could originate from differences in chromosomal axis structure between sexes.

Despite evolutionary conservation of the SC ultrastructure, its constituent protein sequences are divergent between vertebrates and lower eukaryotes[2]. Nevertheless, yeast transverse filament protein Zip1 is approximately the same size as SYCP1 and displays similar patterns of conservation and structure prediction. Thus, it is possible that Zip1 adopts a similar structure and self-assembly mechanism through underlying structural conservation.

The molecular functions of the SC in recombination, crossover formation and interference remain unknown. Nevertheless, we speculate that its three-dimensional structure may direct these processes by regulating enzymatic access to recombination sites. The ability of coiled-coil proteins to transmit conformational changes recursively may further enable the SC to communicate signals along synapsed chromosomes. As our understanding of the SC structure deepens, its molecular functions will gradually be uncovered, ultimately leading to a complete mechanistic understanding of recombination and crossover formation within the functional architecture of the SC.

Accession codes

Crystallographic structure factors and atomic co-ordinates have been deposited in the Protein Data Bank (PDB) under accession numbers 6F5X, 6F62, 6F63 and 6F64.

Acknowledgements

O.R.D. thanks D.W. Sinclair for scientific inspiration and support. We thank Diamond Light Source and the staff of beamlines I02, I04-1 and B21 (proposals mx9948, mx13587, sm14435, sm15580, sm15897 and sm15836). We thank A. Baslé and H. Waller for assistance with X-ray crystallographic and CD data collection, and L. J. Salmon and V. A. Jatikusumo for work in the early stages of this project. I.U. is funded by grants BIO2015-64216-P and MDM2014-0435-01 (MINECO, Spanish Ministry of Economy and Competitiveness). C.M. is supported by a MINECO BES-2015-071397 scholarship associated to the Structural Biology Maria de Maeztu Unit of Excellence. S.M. is supported by a Wellcome Trust Career Re-entry Fellowship (062376). O.R.D. is a Sir Henry Dale Fellow jointly funded by the Wellcome Trust and Royal Society (Grant Number 104158/Z/14/Z).

Author contributions

J.M.D. performed the majority of biochemical, biophysical and crystallographic experiments. O.M.D. performed SAXS experiments and analyses. M.R. crystallised truncated αN-end and analysed αN constructs. C.M. and I.U. solved the αC-end crystal structures. O.R.D. solved the αN-end crystal structures and built/refined all structures. S.M. assisted with initial experiments. J.M.D. and O.R.D. designed experiments; O.R.D. wrote the manuscript.

Competing financial interests

The authors declare no competing interests.

References

1. Zickler, D. & Kleckner, N. Recombination, Pairing, and Synapsis of Homologs during Meiosis. *Cold Spring Harb Perspect Biol* **7**(2015).
2. Page, S.L. & Hawley, R.S. The genetics and molecular biology of the synaptonemal complex. *Annu Rev Cell Dev Biol* **20**, 525-58 (2004).
3. Hunter, N. Meiotic Recombination: The Essence of Heredity. *Cold Spring Harb Perspect Biol* **7**(2015).
4. Baudat, F., Imai, Y. & de Massy, B. Meiotic recombination in mammals: localization and regulation. *Nat Rev Genet* **14**, 794-806 (2013).
5. de Vries, F.A. et al. Mouse Sycp1 functions in synaptonemal complex assembly, meiotic recombination, and XY body formation. *Genes Dev* **19**, 1376-89 (2005).
6. Kouznetsova, A., Benavente, R., Pastink, A. & Hoog, C. Meiosis in mice without a synaptonemal complex. *PLoS One* **6**, e28255 (2011).
7. Handel, M.A. & Schimenti, J.C. Genetics of mammalian meiosis: regulation, dynamics and impact on fertility. *Nat Rev Genet* **11**, 124-36 (2010).
8. Nagaoka, S.I., Hassold, T.J. & Hunt, P.A. Human aneuploidy: mechanisms and new insights into an age-old problem. *Nat Rev Genet* **13**, 493-504 (2012).
9. Westergaard, M. & von Wettstein, D. The synaptinemal complex. *Annu Rev Genet* **6**, 71-110 (1972).
10. Solari, A.J. & Moses, M.J. The structure of the central region in the synaptonemal complexes of hamster and cricket spermatocytes. *J Cell Biol* **56**, 145-52 (1973).
11. Schmekel, K., Skoglund, U. & Daneholt, B. The three-dimensional structure of the central region in a synaptonemal complex: a comparison between rat and two insect species, Drosophila melanogaster and Blaps cribrosa. *Chromosoma* **102**, 682-92 (1993).
12. Schucker, K., Holm, T., Franke, C., Sauer, M. & Benavente, R. Elucidation of synaptonemal complex organization by super-resolution imaging with isotropic resolution. *Proc Natl Acad Sci U S A* **112**, 2029-33 (2015).
13. Meuwissen, R.L. et al. A coiled-coil related protein specific for synapsed regions of meiotic prophase chromosomes. *EMBO J* **11**, 5091-100 (1992).
14. Liu, J.G. et al. Localization of the N-terminus of SCP1 to the central element of the synaptonemal complex and evidence for direct interactions between the N-termini of SCP1 molecules organized head-to-head. *Exp Cell Res* **226**, 11-9 (1996).
15. Schmekel, K. et al. Organization of SCP1 protein molecules within synaptonemal complexes of the rat. *Exp Cell Res* **226**, 20-30 (1996).
16. Hernandez-Hernandez, A. et al. The central element of the synaptonemal complex in mice is organized as a bilayered junction structure. *J Cell Sci* **129**, 2239-49 (2016).
17. Yang, F. et al. Mouse SYCP2 is required for synaptonemal complex assembly and chromosomal synapsis during male meiosis. *J Cell Biol* **173**, 497-507 (2006).
18. Yuan, L. et al. The murine SCP3 gene is required for synaptonemal complex assembly, chromosome synapsis, and male fertility. *Mol Cell* **5**, 73-83 (2000).
19. Syrjanen, J.L., Pellegrini, L. & Davies, O.R. A molecular model for the role of SYCP3 in meiotic chromosome organisation. *Elife* **3**(2014).
20. Yuan, L. et al. Female germ cell aneuploidy and embryo death in mice lacking the meiosis-specific protein SCP3. *Science* **296**, 1115-8 (2002).
21. Syrjanen, J.L. et al. Single-molecule observation of DNA compaction by meiotic protein SYCP3. *Elife* **6**(2017).
22. Schramm, S. et al. A novel mouse synaptonemal complex protein is essential for loading of central element proteins, recombination, and fertility. *PLoS Genet* **7**, e1002088 (2011).

23. Bolcun-Filas, E. et al. Mutation of the mouse Syce1 gene disrupts synapsis and suggests a link between synaptonemal complex structural components and DNA repair. *PLoS Genet* **5**, e1000393 (2009).
24. Costa, Y. et al. Two novel proteins recruited by synaptonemal complex protein 1 (SYCP1) are at the centre of meiosis. *J Cell Sci* **118**, 2755-62 (2005).
25. Gomez, H.L. et al. C14ORF39/SIX6OS1 is a constituent of the synaptonemal complex and is essential for mouse fertility. *Nat Commun* **7**, 13298 (2016).
26. Bolcun-Filas, E. et al. SYCE2 is required for synaptonemal complex assembly, double strand break repair, and homologous recombination. *Journal of Cell Biology* **176**, 741-747 (2007).
27. Hamer, G. et al. Characterization of a novel meiosis-specific protein within the central element of the synaptonemal complex. *Journal of Cell Science* **119**, 4025-4032 (2006).
28. Hamer, G. et al. Progression of meiotic recombination requires structural maturation of the central element of the synaptonemal complex. *J Cell Sci* **121**, 2445-51 (2008).
29. Davies, O.R., Maman, J.D. & Pellegrini, L. Structural analysis of the human SYCE2–TEX12 complex provides molecular insights into synaptonemal complex assembly. *Open Biology* **2**, 120099 (2012).
30. Ollinger, R., Alsheimer, M. & Benavente, R. Mammalian protein SCP1 forms synaptonemal complex-like structures in the absence of meiotic chromosomes. *Mol Biol Cell* **16**, 212-7 (2005).
31. Hanlon, S., Wong, L. & Pack, G.R. Proton equilibria in the minor groove of DNA. *Biophys J* **72**, 291-300 (1997).
32. Seo, E.K., Choi, J.Y., Jeong, J.H., Kim, Y.G. & Park, H.H. Crystal Structure of C-Terminal Coiled-Coil Domain of SYCP1 Reveals Non-Canonical Anti-Parallel Dimeric Structure of Transverse Filament at the Synaptonemal Complex. *PLoS One* **11**, e0161379 (2016).
33. Goldstein, P. Multiple synaptonemal complexes (polycomplexes): origin, structure and function. *Cell Biol Int Rep* **11**, 759-96 (1987).
34. Cahoon, C.K. & Hawley, R.S. Regulating the construction and demolition of the synaptonemal complex. *Nat Struct Mol Biol* **23**, 369-77 (2016).
35. Truebestein, L. & Leonard, T.A. Coiled-coils: The long and short of it. *Bioessays* **38**, 903-16 (2016).
36. Agostinho, A. et al. Sexual dimorphism in the width of the mouse synaptonemal complex. *J Cell Sci* **131**(2018).

Figure Legends

Figure 1

The obligate tetrameric structure of SYCP1.

(**a**) SYCP1 molecules are bioriented within the synaptonemal complex (SC), with midline N-termini and chromosome-bound C-termini, providing a 100 nm separation between chromosome axes. (**b**) Sequence analysis of SYCP1 demonstrating the presence of an α-helical core (amino acids 101-783) that is highly conserved at both ends, flanked by unstructured N- and C-terminal tails. Amino acid conservation was calculated amongst vertebrate sequences. The principal protein constructs analysed in this study are indicated along with their amino acid boundaries. An extensive summary of SYCP1 constructs is provided in Supplementary Fig. 1a and biophysical data are compiled in Supplementary Table 1. (**c**) SEC-MALS analysis; light scattering (LS) and differential refractive index (dRI) are shown as solid and dashed lines respectively, with fitted molecular weights (Mw) plotted as diamonds across elution peaks. SYCP1 αCore (101-783) forms large molecular species of 1-12 MDa, whereas αCore-ΔNtip (112-783) is a 306 kDa tetramer (theoretical tetramer – 320 kDa) consisting of a 68 kDa αN-tetramer (theoretical tetramer – 76 kDa) and 97 kDa αC-dimer (theoretical dimer – 101 kDa). (**d**) SEC-SAXS P(r) distributions of αCore-ΔNtip, αN-tetramer and αC-dimer; maximum dimensions (Dmax) and cross-sectional radii (Rc) are indicated. (**e**) SEC-SAXS P(r) distributions of MBP-αCore-ΔNtip, MBP-αN-tetramer, MBP-αC-dimer and MBP; intra-MBP and inter-MBP peaks are indicated. (**f**) SEC-MALS analysis showing that RecE-αN-tetramer is a 208 kDa tetramer (theoretical tetramer- 214 kDa) and GST-αC-dimer is a 157 kDa dimer (theoretical dimer - 160 kDa). (**g**) Model of the SYCP1 obligate unassembled structure. The SYCP1 α-helical core has a parallel organisation and consists of a 260 Å αN-tetramer that bifurcates into two 645 Å αC-dimer coiled-coils.

Figure 2

Crystal structures of the SYCP1 αN-end head-to-head assembly in open and closed conformations.

(**a**) Crystal structure of SYCP1 αN-end (101-206) demonstrating head-to-head 'dimer of dimers' assembly of two eleven heptad parallel coiled-coils, spanning a total length of 288 Å. The long dimeric coiled-coils are interrupted by a wedge-like structure that splays apart the two α-helices to enable their αN-tip sites to mediate midline head-to-head assembly in an open conformation. The head-to-head interface provides 1,990 $Å^2$ buried surface area in addition to 4,520 $Å^2$ for each coiled-coil dimer alone. (**b**) Crystal structure of truncated SYCP1 αN-end (101-175) demonstrating a similar head-to-head 'dimer of dimers' assembly of two seven heptad parallel coiled-coils, spanning 194 Å, with αN-tips undergoing head-to-head assembly in a closed conformation. The head-to-head interface provides 2,950 $Å^2$ buried surface area in addition to the 2,210 $Å^2$ for each coiled-coil dimer alone. C-terminal interactions of αN-end-truncated chains within the crystal lattice were determined to be artefactual owing to their absence in the αN-end structure and through *in vitro* mutagenesis experiments (M.R. and O.R.D., unpublished data).

Figure 3

Head-to-head assembly interfaces of SYCP1 αN-end.

(**a-c**) Crystal structure of SYCP1 αN-end (101-206). (**a**) A wedge structure formed of residues I116 and W119 splays apart coiled-coil α-helices to enable their head-to-head assembly. (**b-c**) The open assembly is formed of one midline and two lateral interfaces. (**b**) The midline interface (open) is an anti-parallel coiled-coil between symmetry-related chain A copies, with heptad residues L102, V105, L109 and E112. (**c**) The lateral interface (open) is an anti-parallel association of unique chains A and B, formed of coiled-coil and aromatic stacking interactions of residues L102, L109, Y106 and Y110. (**d-f**) Crystal structure of truncated SYCP1 αN-end (101-175). (**d**) Similar to αN-end, a wedge structure of residues I116 and W119 splays apart α-helices to enable their head-to-head assembly. (**e-f**) The closed assembly is formed of a hydrophobic core and interfaces that are analogous to the midline and lateral interfaces of the open conformation. (**e**) The midline interface (closed) is an anti-parallel coiled-coil of heptad residues G101, V105, K108 and E112. (**f**) The lateral interface (closed) is

anti-parallel, consisting of coiled-coil and interlaced aromatic stacking interactions of residues L102, L109, Y106 and Y110. (**g-h**) Cross-sections through the αN-end head-to-head open and closed conformations. (**g**) The open conformation contains no hydrophobic core and is asymmetrical in nature, with midline chain A copies flanked by two copies of chain B. (**h**) The closed conformation is formed of symmetry-related chains and contains a hydrophobic core of residues L102, L109 and I116.

Figure 4

SYCP1 N-terminal self-assembly into higher order structures is mediated by αN-end head-to-head interactions.

(**a-b**) SEC-MALS analysis. (**a**) SYCP1 αN (101-362) (black, left) forms large molecular species of 3-25 MDa, whereas αN-ΔNtip (112-362) (grey) and αN (101-362) V105E L109E (black, right) form tetramers of 118 kDa and 121 kDa respectively (theoretical tetramers – 121 kDa and 126 kDa). (**b**) SYCP1 αN-end, truncated αN-end and αN-end~Ntail are monomeric species of 15 kDa, 10 kDa and 23 kDa respectively (theoretical monomers - 13 kDa, 9 kDa and 20 kDa). (**c**) Model of SYCP1 N-terminal self-assembly. SYCP1 αN-ends splay from αN-tetramers and interact head-to-head in the midline to create a continuous lattice-like assembly. (**d**) SYCP1 N-terminal self-assembly is predicted to be highly cooperative, enabling stable structure formation through a series of individually weak head-to-head associations. This allows transient chromosome associations to be formed and remodelled rapidly, ultimately favouring a single continuous assembly between aligned chromosome axes.

Figure 5

Crystal structure of the SYCP1 C-terminal tetrameric assembly.

(**a**) Crystal structure of SYCP1 αC-end (676-770) in crystal form 1, demonstrating an anti-parallel tetrameric assembly of length 142 Å. The structure includes a central tetrameric interface flanked by

C703 pinch points that lead to lateral four-helical bundles. N- and C-termini are coloured in green and red respectively. (**b**) The central tetrameric interface consists of two stacked layers each containing a hydrogen bonding network of pairs of H717, Q720 and Y721 residues. (**c-d**) The C703 pinch point consists of a parallel dimeric coiled-coil (containing C703) flanked by surrounding anti-parallel chains. (**c**) The parallel dimeric coiled-coil is formed of heptad residues D700, C703, I707, M710 and M714 (**d**) The flanking chains have a distinct angulation at E731 and provide pseudo-cores of loose anti-parallel interactions. (**e-g**) The lateral four-helical bundle (4HB) is formed of a hydrophobic core and anti-parallel interfaces. (**e**) The lateral 4HB type 1 interface is an anti-parallel coiled-coil of heptad residues L679, V682 and K686, L753, K757, L760 and K764. (**f**) The lateral 4HB type 2 interface is an anti-parallel coiled-coil of heptad residues L678, E681, A685, I688 and A692, L745, L749, E752, L756 and E759. (**g**) Cross-section through the lateral 4HB assembly. A hydrophobic core is formed from residues that also contribute to 4HB anti-parallel interfaces and are predicted to mediate the formation of N- and C-terminal parallel dimeric coiled-coils in the non-assembled conformation. L679 and I688 are the only hydrophobic 4HB residues not also implicated in the putative parallel dimeric coiled-coil structure.

Figure 6

SYCP1 αC-end undergoes pH-induced assembly into an anti-parallel tetramer.

(**a**) SEC-MALS analysis. SYCP1 αC-end (676-770) is a 22 kDa dimer at pH 8.0 (grey) (theoretical dimer – 23 kDa) and a 43 kDa tetramer at pH 5.5 (black) (theoretical tetramer – 46 kDa). (**b**) SEC-SAXS P(r) distributions of αC-end at pH 5.5 (black) and pH 8.0 (grey). (**c-d**) SAXS *ab initio* models of the tetrameric and dimeric conformations of SYCP1 αC-end (676-770) at (**c**) pH 5.5 and (**d**) pH 8.0. Averaged models were generated from 20 independent DAMMIF runs with NSD values 0.527 (± 0.014) and 0.513 (± 0.014), and reference model χ^2 values 1.81 and 1.49. The αC-end tetrameric crystal structure and a theoretical dimeric coiled-coil were docked into the respective envelopes. (**e**) SEC-SAXS P(r) distributions of N-terminal, C-terminal and both N- and C-terminal MBP fusions of αC-

end at pH 8.0, alongside MBP-αC-end at pH 5.5. (**f**) SEC-MALS analysis reveals that αC-end tethered dimer forms dimers of 44 kDa and 43 kDa (theoretical dimer of dimers – 47 kDa) at pH 5.5 (black, right) and pH 8.0 (black, left), with an increase in elution volume at pH 5.5. The αC-end (single chain) tetramer at pH 5.5 is shown in grey. (**g**) SEC-SAXS P(r) distributions of the αC-end tethered dimer at pH 5.5 (black) and pH 8.0 (grey). (**h**) SEC-MALS analysis of SYCP1 αC-end extended (676-783) point mutants. H717W Y721F (black) forms 40 kDa tetramers at pH 8.0 (theoretical tetramer – 52 kDa). L679A I688A (grey) fails to undergo pH-induced assembly and remains mostly as a 26 kDa dimer (theoretical dimer – 26 kDa) at pH 4.6.

Figure 7

DNA binding by SYCP1.

(**a**) Surface electrostatic potential of the SYCP1 αC-end crystal structure (red – electronegative; blue – electropositive). The flat surface of the αC-end structure contains five demarcated basic patches that are separated by approximately 30 Å. (**b**) EMSA analysing the ability of SYCP1 αC-end (676-770) to interact with linear double-stranded DNA (dsDNA) at pH 8.0 (top) and pH 5.5 (bottom). Uncropped gel images are shown in Supplementary Data Set 1 (**c**) EMSA of MBP fusions of αC-end~Ctail (640-976), Ctail (784-976), αC-dimer~Ctail (358-976) and αCore~Ctail (101-976) with linear dsDNA at pH 8.0. (**d**) Electron microscopy (EM) analysis of MBP fusions of αC-dimer~Ctail (358-976) and αC-end~Ctail (640-976) in complex with plasmid dsDNA. Scale bars, 50 nm. (**e**) EMSA of refolded full length SYCP1 (1-976) and ΔCtail (1-783) with linear dsDNA at pH 8.0. (**f**) Model of SYCP1 chromosomal axis assembly. SYCP1 molecules are initially recruited to chromosomes through Ctail DNA-binding sites. The close proximity of DNA and/or interactions with chromosome axis proteins then triggers protonation-induced assembly of αC-ends into anti-parallel tetramers that bind DNA and thereby reinforce Ctail interactions. This results in the complete coating of the chromosome axis with SYCP1 molecules linked together through U-shaped assemblies that are anchored to chromosomal DNA.

Figure 8

Meiotic chromosome synapsis through SYCP1 self-assembly.

(**a**) Model of the SYCP1 obligate unassembled structure. The αCore consists of a parallel αN-tetramer that splays into two αC-dimers. The αN-tetramer splays at its N-terminus into αN-end self-assembly sites that lead to unstructured Ntails. The αC-dimers terminate as αC-end self-assembly sites, leading to unstructured Ctails that contain DNA-binding sequences. (**b**) Model of chromosome synapsis by SYCP1. The bifurcating SYCP1 αCore presents pairs of αN-end and αC-end self-assembly sites in the midline and chromosome axis respectively. αN-end sites undergo head-to-head assembly through their αN-tips to provide zipper-like associations that mediate synapsis of SYCP1-coated homologous chromosomes. αC-end sites undergo back-to-back assembly into tetrameric structures that bind directly to DNA within the lateral element and reinforce axis associations of Ctails. Together, these distinct mechanisms of SYCP1 self-assembly generate a supramolecular lattice between meiotic chromosome pairs. (**c**) Concomitant and mutually reinforcing assembly of SYCP1 and central element proteins in SC formation. Initial SYCP1 contacts trigger central element recruitment, enabling growth of the SYCP1 assembly, extending the central element and thereby enabling further SYCP1 growth. (**d**) Model of the mature SC. The central element may provide vertical and longitudinal supports between SYCP1 αN-tetramers to rigidify SYCP1 hemi-lattices and orientate αN-ends for long range cooperative head-to-head assembly. They may also act as transverse bridges that provide direct connections across the midline to reinforce SYCP1 head-to-head interactions. This leads to the formation of a mature SC in which an underlying SYCP1 lattice is stabilised and extended across long distances through central element assembly.

Table 1 Data collection and refinement statistics

	SYCP1 αN-end 101-206 Open conformation (PDB 6F62)	SYCP1 αN-end truncated 101-175 Closed conformation (PDB 6F5X)	SYCP1 αC-end 676-770 Crystal form 1 (PDB 6F63)	SYCP1 αC-end 676-770 Crystal form 2 (PDB 6F64)
Data collection				
Space group	I2	I222	C2	$I4_122$
Cell dimensions				
a, *b*, *c* (Å)	65.67, 37.31, 108.52	28.64, 39.38, 165.77	233.42, 42.85, 43.69	43.38, 43.38, 292.18
α, β, γ (°)	90.00, 106.66, 90.00	90.00, 90.00, 90.00	90.00, 93.61, 90.00	90.00, 90.00, 90.00
Wavelength (Å)	0.9282	1.7712	0.9795	0.9795
Resolution (Å)	34.87–2.06 (2.12–2.06)[a]	41.44–1.91 (1.95–1.91)[a]	116.48–2.15 (2.27–2.15)[a]	42.91–2.48 (2.58–2.48)[a]
R_{merge}	0.071 (0.919)	0.028 (0.678)	0.052 (0.695)	0.080 (2.567)
R_{pim}	0.023 (0.286)	0.017 (0.541)	0.032 (0.429)	0.023 (0.727)
$I / \sigma(I)$	15.0 (1.8)	27.9 (1.8)	12.4 (1.9)	14.8 (1.5)
$CC_{1/2}$	0.999 (0.969)	1.000 (0.839)	0.998 (0.872)	1.000 (0.935)
Completeness (%)	99.9 (100.0)	99.3 (92.1)	97.4 (88.0)	99.8 (99.7)
Redundancy	11.0 (11.4)	5.9 (3.7)	3.6 (3.5)	13.2 (13.2)
Refinement				
Resolution (Å)	27.23–2.07	41.44–1.91	58.26–2.15	39.63–2.49
UCLA anisotropy (Å)	2.1, 2.1, 2.6	1.9, 2.0, 2.1	2.2, 2.3, 2.2	2.9, 2.9, 2.5
No. reflections	12467	6754	21416	4138
R_{work} / R_{free}	0.2264/0.2441	0.2272/0.2392	0.2186/0.2526	0.2251/0.2517
No. atoms	1866	677	3318	806
Protein	1744	633	3143	786
Ligand/ion	18	12	0	4
Water	104	32	175	16
B-factors	42.79	58.4	46.97	60.86
Protein	42.51	57.7	47.30	60.80
Ligand/ion	62.91	83.9	N/A	81.59
Water	44.02	61.7	41.20	58.92
R.m.s. deviations				
Bond lengths (Å)	0.002	0.009	0.004	0.004
Bond angles (°)	0.334	1.020	0.511	0.575

[a]Values in parentheses are for highest-resolution shell.

Online Methods

Recombinant protein expression and purification

Sequences corresponding to regions of human SYCP1 were cloned into pHAT4, pGAT3 or pMAT11 vectors for expression as TEV-cleavable N-terminal His_6-, His_6-GST or His_6-MBP fusion proteins respectively. A list of protein constructs, including sequence boundaries, is provided in Supplementary Fig. 1a and Supplementary Table 1. Constructs were expressed in BL21 (DE3) cells (Novagen®), in 2xYT media, induced with 0.5 mM IPTG for 16 hours at 25°C. Cells were lysed by sonication in 20 mM Tris pH 8.0, 500 mM KCl, and fusion proteins were purified from clarified lysate through consecutive Ni-NTA (Qiagen), amylose (NEB) or glutathione sepharose (GE Healthcare), and HiTrap Q HP (GE Healthcare) ion exchange chromatography. Affinity tags were removed by incubation with TEV protease and cleaved samples were purified by HiTrap Q HP ion exchange chromatography and size exclusion chromatography (HiLoad™ 16/600 Superdex 200, GE Healthcare) in 20 mM Tris pH 8.0, 150 mM KCl, 2 mM DTT. Protein samples were concentrated using Amicon Ultra® 10,000 MWCO centrifugal filter units (Millipore), and were stored at -80˚C following flash-freezing in liquid nitrogen. Protein samples were analysed by SDS-PAGE with Coomassie staining, and concentrations were determined by UV spectroscopy using a Cary 60 UV spectrophotometer (Agilent) with extinction coefficients and molecular weights calculated by ProtParam (http://web.expasy.org/protparam/).

Purification of refolded full length SYCP1

Full-length human SYCP1 (amino acids 1-976) was expressed using a pHAT4 vector in Rosetta (DE3) cells, grown in 2xYT media and induced with 0.5 mM IPTG for 3 hours at 37°C. Cells were lysed by sonication in 20 mM Tris pH 8.0, 500 mM NaCl and the insoluble fraction pelleted through centrifugation at 40,000 g for 30 minutes. The resultant pellet was washed in 20 mM Tris pH 8.0, 500 mM NaCl prior to solubilisation in 20 mM Tris pH 8.0, 500 mM NaCl, 8M urea pH 8.0. DNA-containing hydrogels were formed by consecutive dialysis into 20 mM Tris pH 8.0, 500 mM NaCl, 500 mM L-

arginine pH 8.0, followed by 20 mM Tris pH 8.0, 500 mM NaCl. Soluble SYCP1 was produced by removal of DNA from the denatured material through ion exchange chromatography, prior to the refolding protocol through dialysis, as described above.

Circular dichroism (CD) spectroscopy

Far UV circular dichroism (CD) spectroscopy data were collected on a Jasco J-810 spectropolarimeter (Institute for Cell and Molecular Biosciences, Newcastle University). CD spectra were recorded in 10mM Na_2HPO_4/ NaH_2PO_4 pH 7.5, at protein concentrations between 0.1-0.5 mg/ml, using a 0.2 mm pathlength quartz cuvette (Hellma), at 0.2 nm intervals between 260 and 185 nm at 4°C. Spectra were averaged across nine accumulations, corrected for buffer signal, smoothed and converted to mean residue ellipticity ([θ]) (x1000 $deg.cm^2.dmol^{-1}.residue^{-1}$). Deconvolution was performed using the CDSSTR algorithm of the Dichroweb server (http://dichroweb.cryst.bbk.ac.uk)[37]. CD thermal denaturation was performed in 20 mM Tris pH 8.0, 150 mM KCl, 2 mM DTT, at protein concentrations between 0.1-0.4 mg/ml, using a 1 mm pathlength quartz cuvette (Hellma). Data were recorded at 222 nm, between 5°C and 95°C, at 0.5°C intervals with ramping rate of 2°C per minute, and were converted to mean residue ellipticity ($[\theta_{222}]$) and plotted as % unfolded ($[\theta]_{222,x}$-$[\theta]_{222,5}$)/($[\theta]_{222,95}$-$[\theta]_{222,5}$). Melting temperatures (Tm) were estimated as the points at which samples are 50% unfolded. SYCP1 αC-end constructs were also analysed in 50 mM NaOAc pH 5.5 or 4.6, 150 mM KCl.

Size-exclusion chromatography multi-angle light scattering (SEC-MALS)

The absolute molar masses of SYCP1 constructs were determined by size-exclusion chromatography multi-angle light scattering (SEC-MALS). Protein samples at >1 mg/ml were loaded onto a Superdex™ 200 Increase 10/300 GL size exclusion chromatography column (GE Healthcare) in 20 mM Tris pH 8.0, 150 mM KCl, 2 mM DTT, at 0.5 ml/min using an ÄKTA™ Pure (GE Healthcare). SYCP1 αC-end constructs were also analysed in 50 mM NaOAc pH 5.5 or 4.6, 150 mM KCl, 2 mM DTT. The column

718 outlet was fed into a DAWN® HELEOS™ II MALS detector (Wyatt Technology), followed by an
719 Optilab® T-rEX™ differential refractometer (Wyatt Technology). Light scattering and differential
720 refractive index data were collected and analysed using ASTRA® 6 software (Wyatt Technology).
721 Molecular weights and estimated errors were calculated across eluted peaks by extrapolation from
722 Zimm plots using a dn/dc value of 0.1850 ml/g. SEC-MALS data are presented with light scattering
723 (LS) and differential refractive index (dRI) profiles, with fitted molecular weights (M_W) plotted across
724 elution peaks.
725
726 **Electrophoretic mobility shift assay (EMSA)**
727 SYCP1 protein constructs were incubated with 25 or 32 µM (per base pair) 470 or 75 bp linear dsDNA
728 substrate at concentrations indicated, in 20 mM Tris pH 8.0, 150 mM KCl or 50 mM NaOAc pH 5.5,
729 150 mM KCl, for 5 minutes at 4°C. Glycerol was added at a final concentration of 3% and samples
730 were analysed by electrophoresis on a 0.5% (w/v) agarose gel in 0.5x TBE pH 8.0 or 25 mM GABA pH
731 5.5 at 20V for 4 hours at 4°C. DNA was detected by SYBR™ safe (ThermoFisher).
732
733 **Size-exclusion chromatography small-angle X-ray scattering (SEC-SAXS)**
734 SEC-SAXS experiments were performed at beamline B21 of the Diamond Light Source synchrotron
735 facility (Oxfordshire, UK). Protein samples at concentrations >10 mg/ml were loaded onto a
736 Superdex™ 200 Increase 10/300 GL size exclusion chromatography column (GE Healthcare) in 20
737 mM Tris pH 8.0, 150 mM KCl at 0.5 ml/min using an Agilent 1200 HPLC system. SYCP1 αC-end
738 constructs were also analysed in 50 mM NaOAc pH 5.5 or 4.6, 150 mM KCl. The column outlet was
739 fed into the experimental cell, and SAXS data were recorded at 12.4 keV, detector distance 4.014 m,
740 in 3.0 s frames. Data were subtracted and averaged, and analysed for Guinier region Rg and cross-
741 sectional Rg (Rc) using ScÅtter 3.0 (http://www.bioisis.net). Approximate parameters for real space
742 analysis were determined using the server www.bayesapp.org, and P(r) distributions fitted using
743 PRIMUS[38]. *Ab initio* modelling was performed using DAMMIF[39] run in interactive mode with random

744 chain selected as expected shape. 10-20 independent runs were performed and averaged. Crystal
745 structures and models were docked into DAMAVER molecular envelopes using SUPCOMB[40].
746
747 **Electron Microscopy**
748 Electron microscopy (EM) was performed using an FEI Philips CM100 transmission electron
749 microscope at the Electron Microscopy Research Services, Newcastle University. MBP fusion SYCP1
750 samples at 10 μM were incubated with 100 μM (per base pair) plasmid double-stranded DNA in 20
751 mM Tris pH 8.0, 250 mM KCl for 10 minutes, and applied to carbon-coated EM grids. Negative
752 staining was performed using 2% (wt/vol) uranyl acetate.
753
754 **Protein crystallisation and X-ray structure solution of SYCP1 αN-end (101-206)**
755 SYCP1 αN-end (101-206) protein crystals were obtained through vapour diffusion in hanging drops,
756 by mixing 200 nl of protein at 10 mg/ml with 100 nl of crystallisation solution (100 mM MES pH 6.0,
757 40% (v/v) MPD) and equilibrating at 4°C for 4-9 days. Crystals were flash frozen in liquid nitrogen. X-
758 ray diffraction data were collected at 0.9282 Å, 100 K, as 2000 consecutive 0.10° frames of 0.050 s
759 exposure on a Pilatus 6M detector at beamline I04-1 of the Diamond Light Source synchrotron
760 facility (Oxfordshire, UK). Data were indexed and integrated in XDS[41] using AutoPROC[42]; datasets
761 from three crystals were scaled together using XSCALE[43] and then merged in Aimless[44]. Crystals
762 belong to monoclinic spacegroup I2 (cell dimensions a = 65.67 Å, b = 37.31 Å, c = 108.52 Å, α = 90°, β
763 = 106.66°, γ = 90°), with two SYCP1 chains per asymmetric unit. Data were corrected for anisotropy
764 using the UCLA diffraction anisotropy server (https://services.mbi.ucla.edu/anisoscale/)[45], imposing
765 anisotropic limits of 2.1 Å, 2.1 Å, 2.6 Å, with principal components of 24.09 $Å^2$, 6.01 $Å^2$ and -20.19 $Å^2$.
766 Structure solution was achieved using AMPLE[46] on the CCP4 online web server
767 (https://www.ccp4.ac.uk/ccp4online/), through molecular replacement of Quark *ab initio* model
768 decoys[47], with auto-tracing and rebuilding in SHELX E and ARP/wARP. Phase improvement was
769 achieved through iterative re-building by PHENIX Autobuild[48]. The structure was completed through

manual model building in Coot and refinement using PHENIX refine[48], with the addition of two 2-methyl-2,4-pentanediol (MPD) ligands and two chloride ions. Refinement was performed using isotropic atomic displacement parameters with riding hydrogens. The structure was refined against anisotropy corrected 2.07 Å data to R and R_{free} values of 0.2264 and 0.2441 respectively, with 100% of residues within the favoured regions of the Ramachandran plot, clashscore of 3.05 and overall MolProbity score of 1.10.

Protein crystallisation and X-ray structure solution of truncated SYCP1-αN-end (101-175)

SYCP1 αN-end-tr (101-175) protein crystals were obtained through vapour diffusion in hanging drops, by mixing 1 µl of protein at 10 mg/ml with 1 µl of crystallisation solution (140 mM NaCl, 70 mM Na/K phosphate pH 6.2, 35% (v/v) PEG200) and equilibrating at 20°C for 4-9 days. Crystals were soaked for 30 minutes in crystallisation solution containing 40% (v/v) PEG200 and 100 mM NaI, prior to flash freezing in liquid nitrogen. X-ray diffraction data were collected at 1.7712 Å, 100 K, as 2000 consecutive 0.10° frames of 0.050 s exposure on a Pilatus 6M detector at beamline I02 of the Diamond Light Source synchrotron facility (Oxfordshire, UK). Data were indexed, integrated and scaled in XDS[41] and XSCALE[43], and merged in Aimless[44]. Crystals belong to orthorhombic spacegroup I222 (cell dimensions a = 28.64 Å, b = 39.38 Å, c = 165.77 Å, α = 90°, β = 90°, γ = 90°), with one SYCP1 chain per asymmetric unit. SAD structure solution was achieved through identification of five putative iodide sites and secondary structure auto-tracing by SHELX C/D/E, utilising the HKL2MAP interface[49]. Phase improvement was achieved through iterative re-building by PHENIX Autobuild[48]. Data were corrected for anisotropy using the UCLA diffraction anisotropy server (https://services.mbi.ucla.edu/anisoscale/)[45], imposing anisotropic limits of 1.9 Å, 2.0 Å, 2.1 Å, with principal components of 13.25 $Å^2$, 0.78 $Å^2$ and -14.08 $Å^2$. The structure was completed through manual model building in Coot and refinement using PHENIX refine[48], with the truncation to two iodide sites (based on anomalous difference map peaks) and the addition of a triethylene glycol ligand (PGE). Refinement was performed using isotropic atomic displacement parameters with five

TLS groups. The structure was refined against anisotropy corrected 1.91 Å data to R and R_{free} values of 0.2272 and 0.2392 respectively, with 100% of residues within the favoured regions of the Ramachandran plot, clashscore of 6.77 and overall MolProbity score of 1.37.

Protein crystallisation and X-ray structure solution of SYCP1 αC-end (676-770) crystal form 1

SYCP1 αC-end (676-770) protein crystals were obtained through vapour diffusion in hanging drops, by mixing 100 nl of protein at 31 mg/ml with 100 nl of crystallisation solution (3.5 M sodium formate pH 7.0) and equilibrating at 20°C for 2 months. Crystals were soaked in a cryoprotectant solution of 6 M sodium formate pH 7.0 and flash frozen in liquid nitrogen. X-ray diffraction data were collected at 0.9795 Å, 100 K, as 2000 consecutive 0.10° frames of 0.080 s exposure on a Pilatus 6M detector at beamline I02 of the Diamond Light Source synchrotron facility (Oxfordshire, UK). Data were indexed and integrated in XDS[41], and scaled and merged in Aimless[44], using AutoPROC[42]. Crystals belong to monoclinic spacegroup C2 (cell dimensions a = 233.42 Å, b = 42.85 Å, c = 43.69 Å, α = 90°, β = 93.61°, γ = 90°), with four SYCP1 chains per asymmetric unit. Structure solution was achieved through fragment-based molecular replacement using ARCIMBOLDO_SHREDDER[50], a program that derives small models from distant homologs, decomposes and refines the fragments against PHASER's[51] gyre and gimble functions[52], and combines partial solutions[53] for expansion through density modification and main chain tracing with SHELXE[54] to generate the full structure. The SYCP1-αC-end $I4_122$ structure (crystal form 2) was used as a starting template for generating 74 models containing 99 amino acids each. A phase set combining 25 partial solutions was expanded into a full solution, recognisable by a correlation coefficient of 48.2%. Phase improvement was achieved through iterative re-building by PHENIX Autobuild[48]. Data were corrected for anisotropy using the UCLA diffraction anisotropy server (https://services.mbi.ucla.edu/anisoscale/)[45], imposing anisotropic limits of 2.2 Å, 2.3 Å, 2.2 Å, with principal components of 18.46 $Å^2$, 3.44 $Å^2$ and -21.90 $Å^2$. The structure was completed through manual model building in Coot and refinement using PHENIX refine[48]. Refinement was performed using isotropic atomic displacement parameters with seven TLS

groups per chain. The structure was refined against anisotropy corrected 2.15 Å data to R and R_{free} values of 0.2186 and 0.2526 respectively, with 100% of residues within the favoured regions of the Ramachandran plot, clashscore of 6.86 and overall MolProbity score of 1.38.

Protein crystallisation and X-ray structure solution of SYCP1 αC-end (676-770) crystal form 2

SYCP1 αC-end (676-770) protein crystals were obtained through vapour diffusion in hanging drops, by mixing 100 nl of protein at 15 mg/ml with 100 nl of crystallisation solution (0.1 M sodium cacodylate pH 6.5, 1.4M sodium acetate) and equilibrating at 20°C for 2 months. Crystals were soaked in a cryoprotectant solution of 0.1 M sodium cacodylate pH 6.5, 1.4 M sodium acetate, 20% PEG400 and flash frozen in liquid nitrogen. X-ray diffraction data were collected at 0.9795 Å, 100 K, as 2000 consecutive 0.10° frames of 0.080 s exposure on a Pilatus 6M detector at beamline I02 of the Diamond Light Source synchrotron facility (Oxfordshire, UK). Data were indexed and integrated in XDS[41] using AutoPROC[42], scaled in XSCALE[43] and scaled merged in Aimless[44]. Crystals belong to tetragonal spacegroup $I4_122$ (cell dimensions a = 43.38 Å, b = 43.38 Å, c = 292.18 Å, α = 90°, β = 90°, γ = 90°), with one SYCP1 chain per asymmetric unit. Structure solution was achieved through fragment-based molecular replacement using ARCIMBOLDO_LITE[55]. Substructures made up of two ideal polyalanine helices of 30 residues each were located with PHASER, profiting from its features for small fragments, and were extended with SHELXE within the Arcimboldo mode for coiled coil structures[56]. A correct solution was identified by a SHELXE Correlation Coefficient of 40.5%. Phase improvement was achieved through iterative re-building by PHENIX Autobuild[48]. Data were corrected for anisotropy using the UCLA diffraction anisotropy server (https://services.mbi.ucla.edu/anisoscale/)[45], imposing anisotropic limits of 2.9 Å, 2.9 Å, 2.5 Å, with principal components of 16.05 $Å^2$, 16.05 $Å^2$ and -32.09 $Å^2$. The structure was completed through manual model building in Coot and refinement using PHENIX refine[48], with the addition of one acetate ligand. Refinement was performed using isotropic atomic displacement parameters with riding hydrogens. The structure was refined against anisotropy corrected 2.49 Å data to R and R_{free}

values of 0.2251 and 0.2517 respectively, with 100% of residues within the favoured regions of the Ramachandran plot, clashscore of 1.24 and overall MolProbity score of 0.84.

Protein sequence and structure analysis

Conservation of SYCP1 amongst vertebrate sequences was calculated as per residue scores for the full SYCP1 sequence and the αC-end structure by ConSurf (http://consurf.tau.ac.il/), and secondary structure prediction was performed by JNet (http://www.compbio.dundee.ac.uk/www-jpred/). Protein structures were superposed and rsmd values calculated by PHENIX superpose[48]. Structural assemblies were analysed by PISA. Molecular structure images were generated using the PyMOL Molecular Graphics System, Version 1.3 Schrödinger, LLC.

Data availability

Crystallographic structure factors and atomic co-ordinates have been deposited in the Protein Data Bank (PDB) under accession numbers 6F5X, 6F62, 6F63 and 6F64. Uncropped gel images are shown in Supplementary Data Set 1. All other data are available from the corresponding author upon reasonable request. A Life Sciences Reporting Summary for this article is available.

Methods-only references

37. Whitmore, L. & Wallace, B.A. Protein secondary structure analyses from circular dichroism spectroscopy: methods and reference databases. *Biopolymers* **89**, 392-400 (2008).
38. P.V.Konarev, V.V.V., A.V.Sokolova, M.H.J.Koch, D. I. Svergun. PRIMUS - a Windows-PC based system for small-angle scattering data analysis. *J Appl Cryst.* **36**, 1277-1282 (2003).
39. Franke, D. & Svergun, D.I. DAMMIF, a program for rapid ab-initio shape determination in small-angle scattering. *J Appl Crystallogr* **42**, 342-346 (2009).
40. Kozin, M.B. & Svergun, D.I. Automated matching of high- and low-resolution structural models. *Journal of Applied Crystallography* **34**, 33-41 (2001).
41. Kabsch, W. Xds. *Acta Crystallogr D Biol Crystallogr* **66**, 125-32 (2010).
42. Vonrhein, C. et al. Data processing and analysis with the autoPROC toolbox. *Acta Crystallogr D Biol Crystallogr* **67**, 293-302 (2011).
43. Diederichs, K., McSweeney, S. & Ravelli, R.B. Zero-dose extrapolation as part of macromolecular synchrotron data reduction. *Acta Crystallogr D Biol Crystallogr* **59**, 903-9 (2003).
44. Evans, P.R. An introduction to data reduction: space-group determination, scaling and intensity statistics. *Acta Crystallogr D Biol Crystallogr* **67**, 282-92 (2011).
45. Strong, M. et al. Toward the structural genomics of complexes: crystal structure of a PE/PPE protein complex from Mycobacterium tuberculosis. *Proc Natl Acad Sci U S A* **103**, 8060-5 (2006).
46. Bibby, J., Keegan, R.M., Mayans, O., Winn, M.D. & Rigden, D.J. AMPLE: a cluster-and-truncate approach to solve the crystal structures of small proteins using rapidly computed ab initio models. *Acta Crystallogr D Biol Crystallogr* **68**, 1622-31 (2012).
47. Xu, D. & Zhang, Y. Ab initio protein structure assembly using continuous structure fragments and optimized knowledge-based force field. *Proteins* **80**, 1715-35 (2012).
48. Adams, P.D. et al. PHENIX: a comprehensive Python-based system for macromolecular structure solution. *Acta Crystallogr D Biol Crystallogr* **66**, 213-21 (2010).
49. Pape, T. & Schneider, T.R. HKL2MAP: a graphical user interface for macromolecular phasing with SHELX programs. *Journal of Applied Crystallography* **37**, 843-844 (2004).
50. Millan, C. et al. Exploiting distant homologues for phasing through the generation of compact fragments, local fold refinement and partial solution combination. *Acta Crystallogr D Struct Biol* **74**, 290-304 (2018).
51. McCoy, A.J. et al. Phaser crystallographic software. *Journal of Applied Crystallography* **40**, 658-674 (2007).
52. McCoy, A.J. et al. Gyre and gimble: a maximum-likelihood replacement for Patterson correlation refinement. *Acta Crystallogr D Struct Biol* **74**, 279-289 (2018).
53. Millan, C. et al. Combining phase information in reciprocal space for molecular replacement with partial models. *Acta Crystallogr D Biol Crystallogr* **71**, 1931-45 (2015).
54. Uson, I. & Sheldrick, G.M. An introduction to experimental phasing of macromolecules illustrated by SHELX; new autotracing features. *Acta Crystallogr D Struct Biol* **74**, 106-116 (2018).
55. Rodriguez, D.D. et al. Crystallographic ab initio protein structure solution below atomic resolution. *Nature Methods* **6**, 651-U39 (2009).
56. Caballero, I. et al. ARCIMBOLDO on coiled coils. *Acta Crystallogr D Struct Biol* **74**, 194-204 (2018).

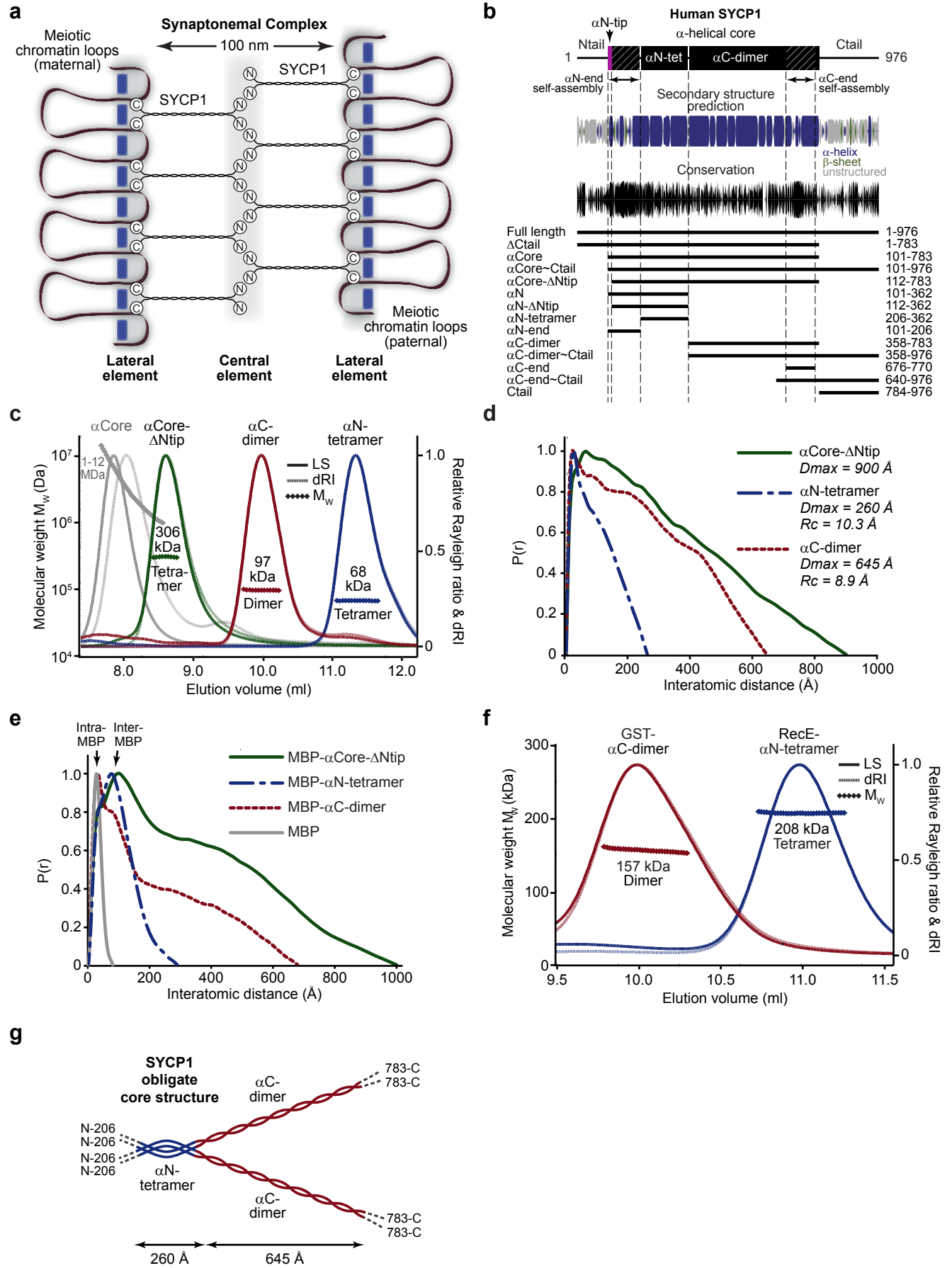
a
Synaptonemal Complex
100 nm
Meiotic chromatin loops (maternal)
SYCP1
SYCP1
Meiotic chromatin loops (paternal)
Lateral element
Central element
Lateral element
b
Human SYCP1
αN-tip
α-helical core
Ntail
Ctail
1
976
αN-tet
αC-dimer
αN-end self-assembly
αC-end self-assembly
Secondary structure prediction
α-helix
β-sheet
unstructured
Conservation
Full length 1-976
ΔCtail 1-783
αCore 101-783
αCore~Ctail 101-976
αCore-ΔNtip 112-783
αN 101-362
αN-ΔNtip 112-362
αN-tetramer 206-362
αN-end 101-206
αC-dimer 358-783
αC-dimer~Ctail 358-976
αC-end 676-770
αC-end~Ctail 640-976
Ctail 784-976
c
αCore
αCore-ΔNtip
αC-dimer
αN-tetramer
1-12 MDa
306 kDa Tetra-mer
97 kDa Dimer
68 kDa Tetramer
LS
dRI
Mw
Molecular weight Mw (Da)
Relative Rayleigh ratio & dRI
Elution volume (ml)
d
αCore-ΔNtip
Dmax = 900 Å
αN-tetramer
Dmax = 260 Å
Rc = 10.3 Å
αC-dimer
Dmax = 645 Å
Rc = 8.9 Å
P(r)
Interatomic distance (Å)
e
Intra-MBP
Inter-MBP
MBP-αCore-ΔNtip
MBP-αN-tetramer
MBP-αC-dimer
MBP
P(r)
Interatomic distance (Å)
f
GST-αC-dimer
RecE-αN-tetramer
157 kDa Dimer
208 kDa Tetramer
LS
dRI
Mw
Molecular weight Mw (kDa)
Relative Rayleigh ratio & dRI
Elution volume (ml)
g
SYCP1 obligate core structure
αC-dimer
783-C
783-C
N-206
N-206
N-206
N-206
αN-tetramer
αC-dimer
783-C
783-C
260 Å
645 Å

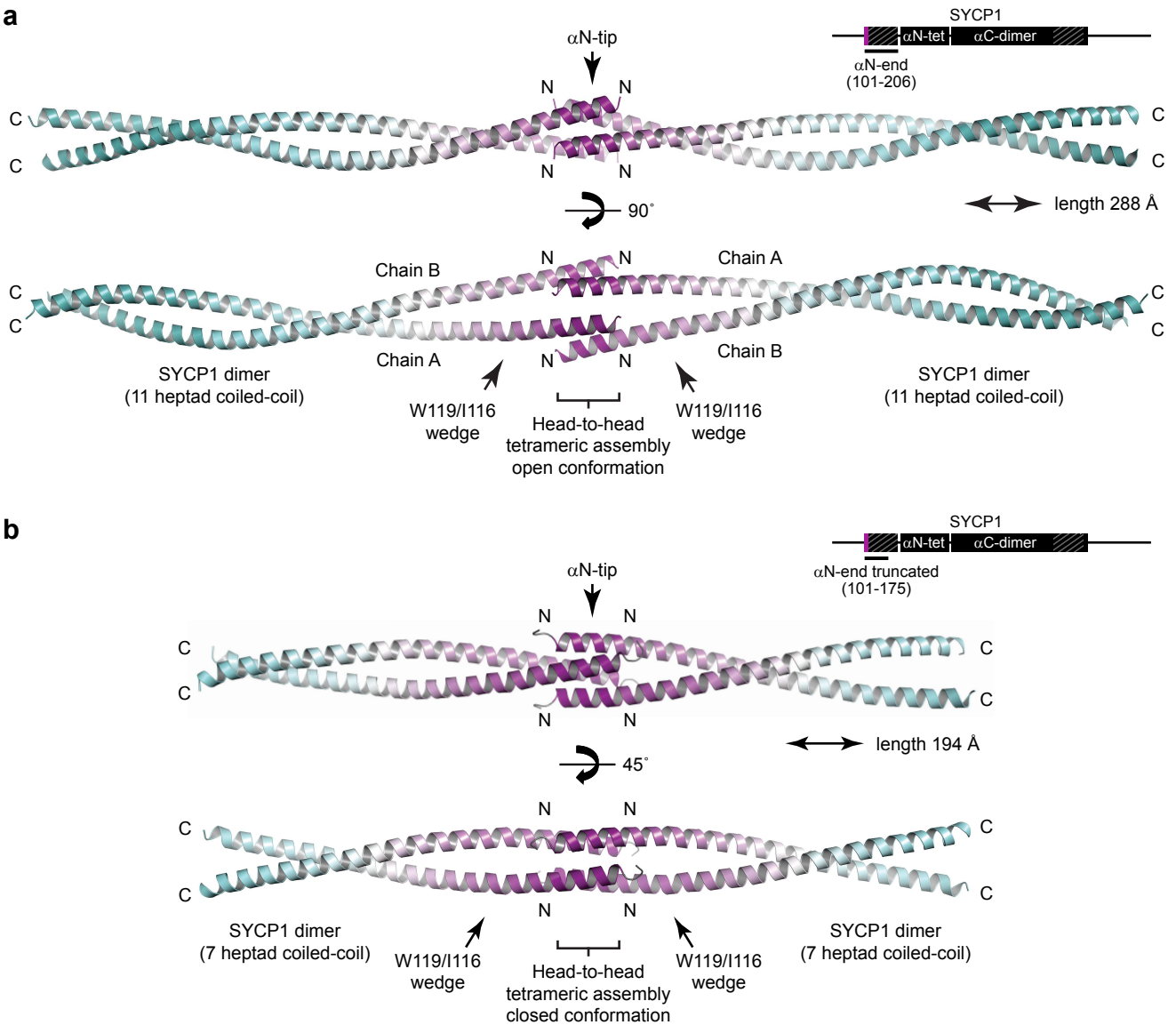
a
SYCP1
αN-tip
αN-tet
αC-dimer
αN-end
(101-206)
N
N
C
C
90˚
length 288 Å
Chain B
Chain A
SYCP1 dimer
(11 heptad coiled-coil)
W119/I116
wedge
Head-to-head
tetrameric assembly
open conformation
b
SYCP1
αN-tip
αN-tet
αC-dimer
αN-end truncated
(101-175)
45˚
length 194 Å
SYCP1 dimer
(7 heptad coiled-coil)
W119/I116
wedge
Head-to-head
tetrameric assembly
closed conformation

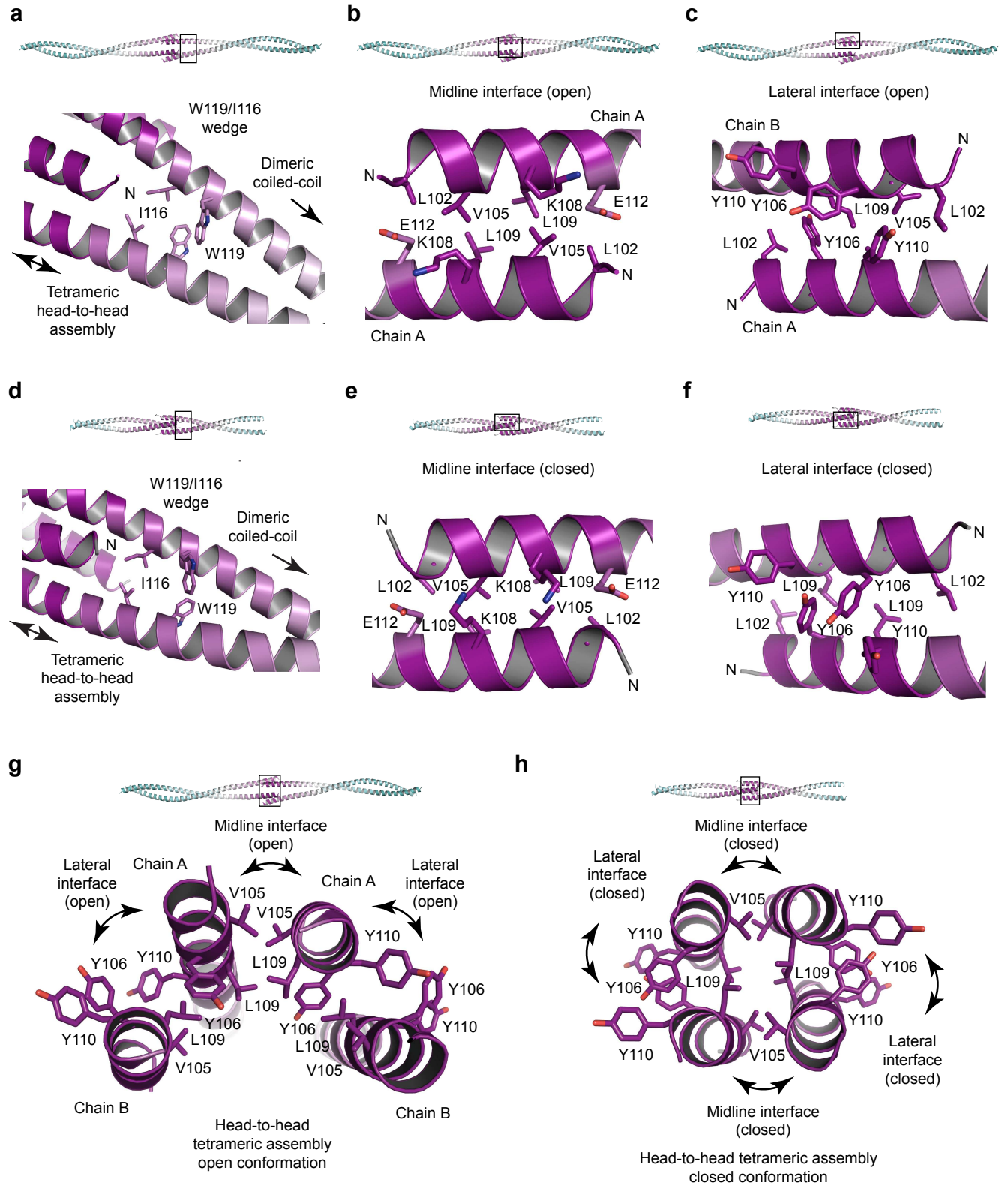
a
W119/I116
wedge
Dimeric
coiled-coil
N
I116
W119
Tetrameric
head-to-head
assembly
b
Midline interface (open)
Chain A
N
L102
V105
K108
E112
L109
E112
K108
L109
V105
L102
N
Chain A
c
Lateral interface (open)
Chain B
N
Y110
Y106
L109
L102
V105
L102
Y106
Y110
N
Chain A
d
W119/I116
wedge
Dimeric
coiled-coil
N
I116
W119
Tetrameric
head-to-head
assembly
e
Midline interface (closed)
N
L102
V105
K108
L109
E112
E112
L109
K108
V105
L102
N
f
Lateral interface (closed)
N
Y110
L109
Y106
L102
L109
L102
Y106
Y110
N
g
Midline interface
(open)
Lateral
interface
(open)
Chain A
Chain A
Lateral
interface
(open)
V105
V105
Y110
Y106
Y110
L109
Y106
L109
Y110
L109
Y106
Y106
Y110
L109
V105
V105
Chain B
Chain B
Head-to-head
tetrameric assembly
open conformation
h
Midline interface
(closed)
Lateral
interface
(closed)
V105
Y110
Y110
Y106
L109
L109
Y106
Y110
Y110
V105
Lateral
interface
(closed)
Midline interface
(closed)
Head-to-head tetrameric assembly
closed conformation

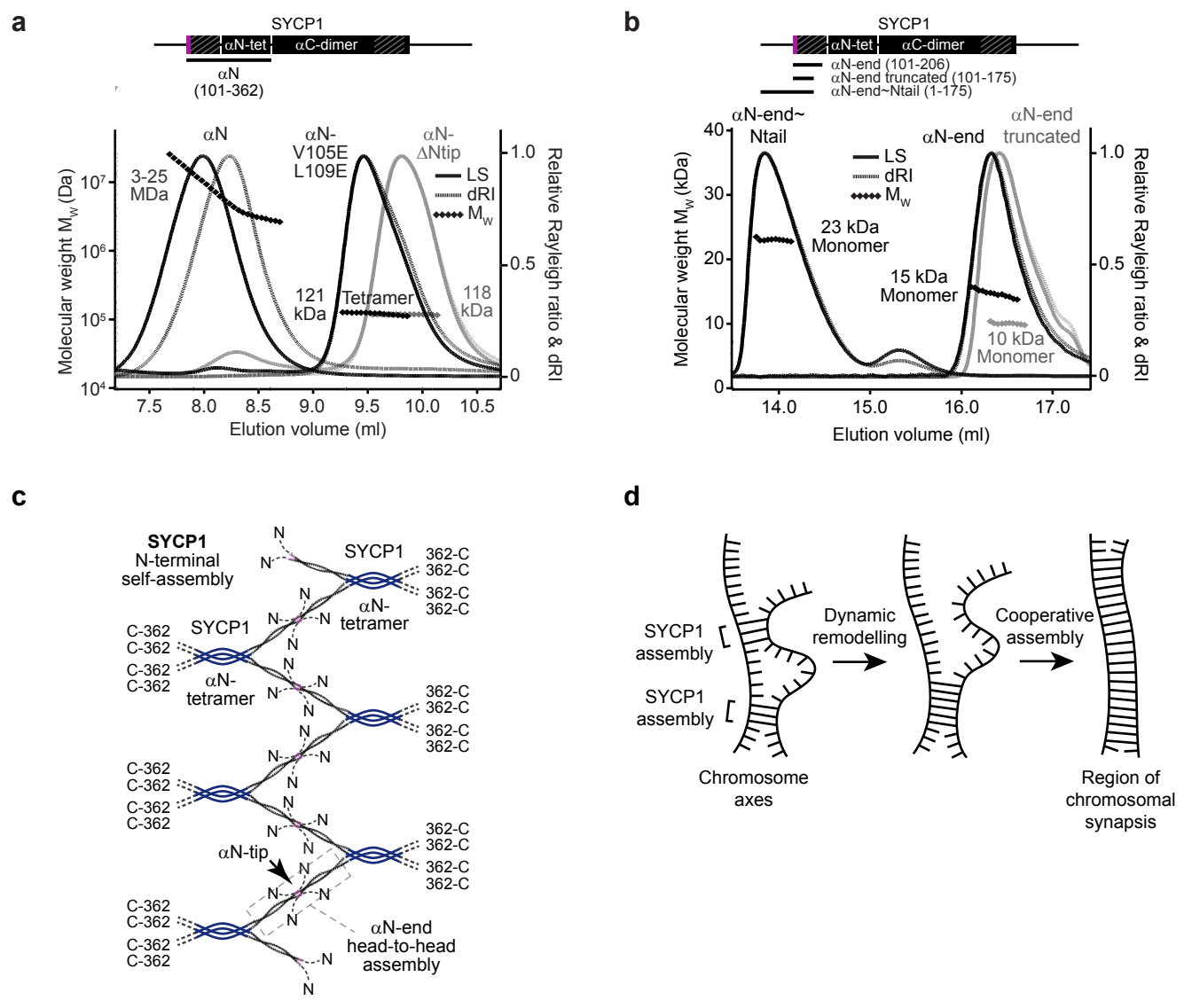
a
SYCP1
αN-tet
αC-dimer
αN
(101-362)
αN
αN-
V105E
L109E
αN-
ΔNtip
LS
dRI
M_w
3-25
MDa
121
kDa
Tetramer
118
kDa
Molecular weight M_w (Da)
Relative Rayleigh ratio & dRI
Elution volume (ml)
b
SYCP1
αN-tet
αC-dimer
αN-end (101-206)
αN-end truncated (101-175)
αN-end~Ntail (1-175)
αN-end~
Ntail
αN-end
αN-end
truncated
LS
dRI
M_w
23 kDa
Monomer
15 kDa
Monomer
10 kDa
Monomer
Molecular weight M_w (kDa)
Relative Rayleigh ratio & dRI
Elution volume (ml)
c
SYCP1
N-terminal
self-assembly
SYCP1
αN-
tetramer
SYCP1
αN-
tetramer
αN-tip
αN-end
head-to-head
assembly
362-C
C-362
d
SYCP1
assembly
SYCP1
assembly
Dynamic
remodelling
Cooperative
assembly
Chromosome
axes
Region of
chromosomal
synapsis

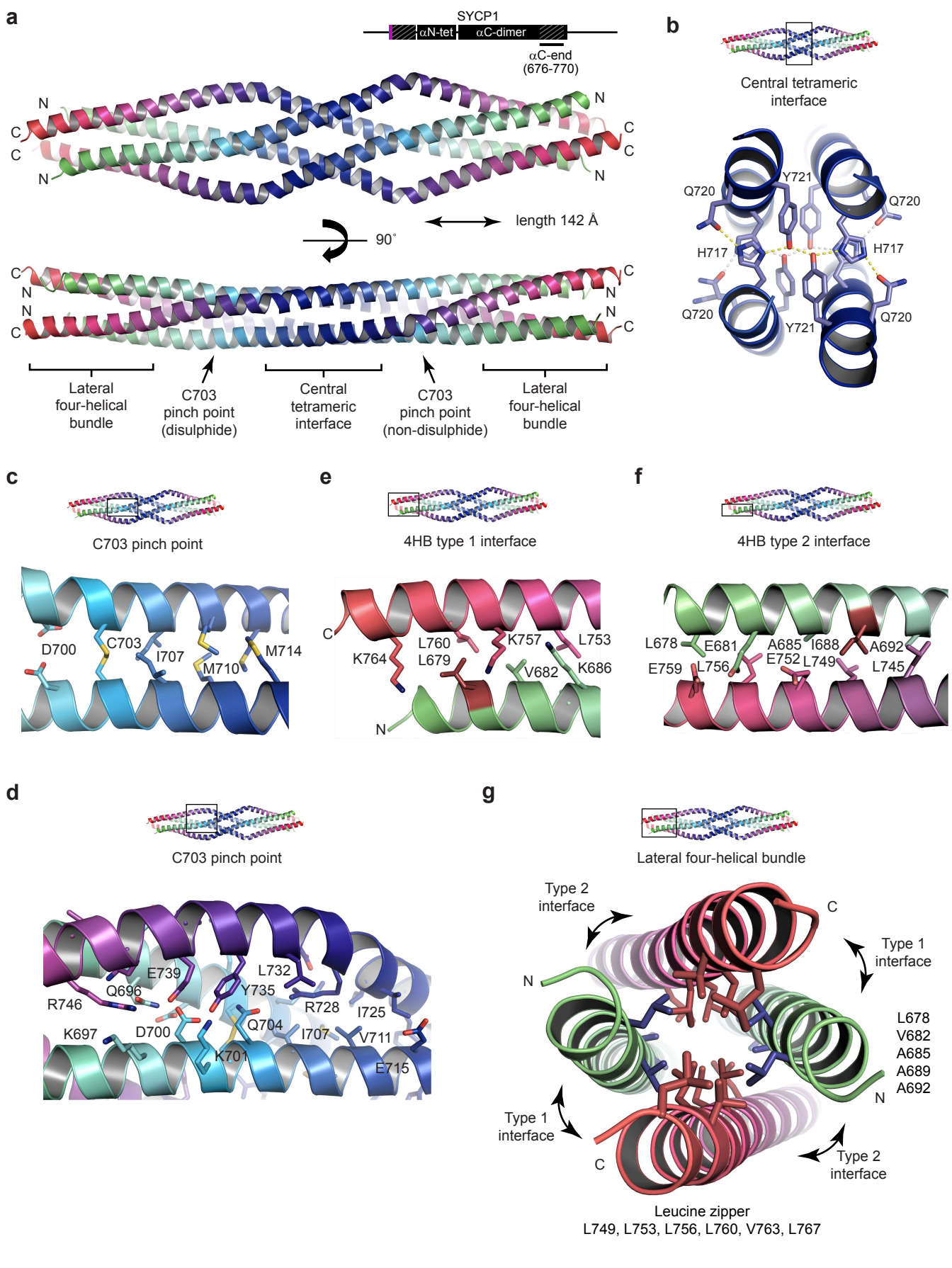
a
SYCP1
αN-tet
αC-dimer
αC-end
(676-770)
N
C
length 142 Å
90˚
Lateral four-helical bundle
C703 pinch point (disulphide)
Central tetrameric interface
C703 pinch point (non-disulphide)
Lateral four-helical bundle
b
Central tetrameric interface
Q720
Y721
H717
c
C703 pinch point
D700
C703
I707
M710
M714
e
4HB type 1 interface
K764
L760
L679
K757
L753
V682
K686
f
4HB type 2 interface
L678
E681
A685
I688
A692
E759
L756
E752
L749
L745
d
C703 pinch point
R746
E739
Q696
L732
Y735
R728
I725
K697
D700
Q704
I707
V711
K701
E715
g
Lateral four-helical bundle
Type 2 interface
Type 1 interface
L678
V682
A685
A689
A692
Leucine zipper
L749, L753, L756, L760, V763, L767

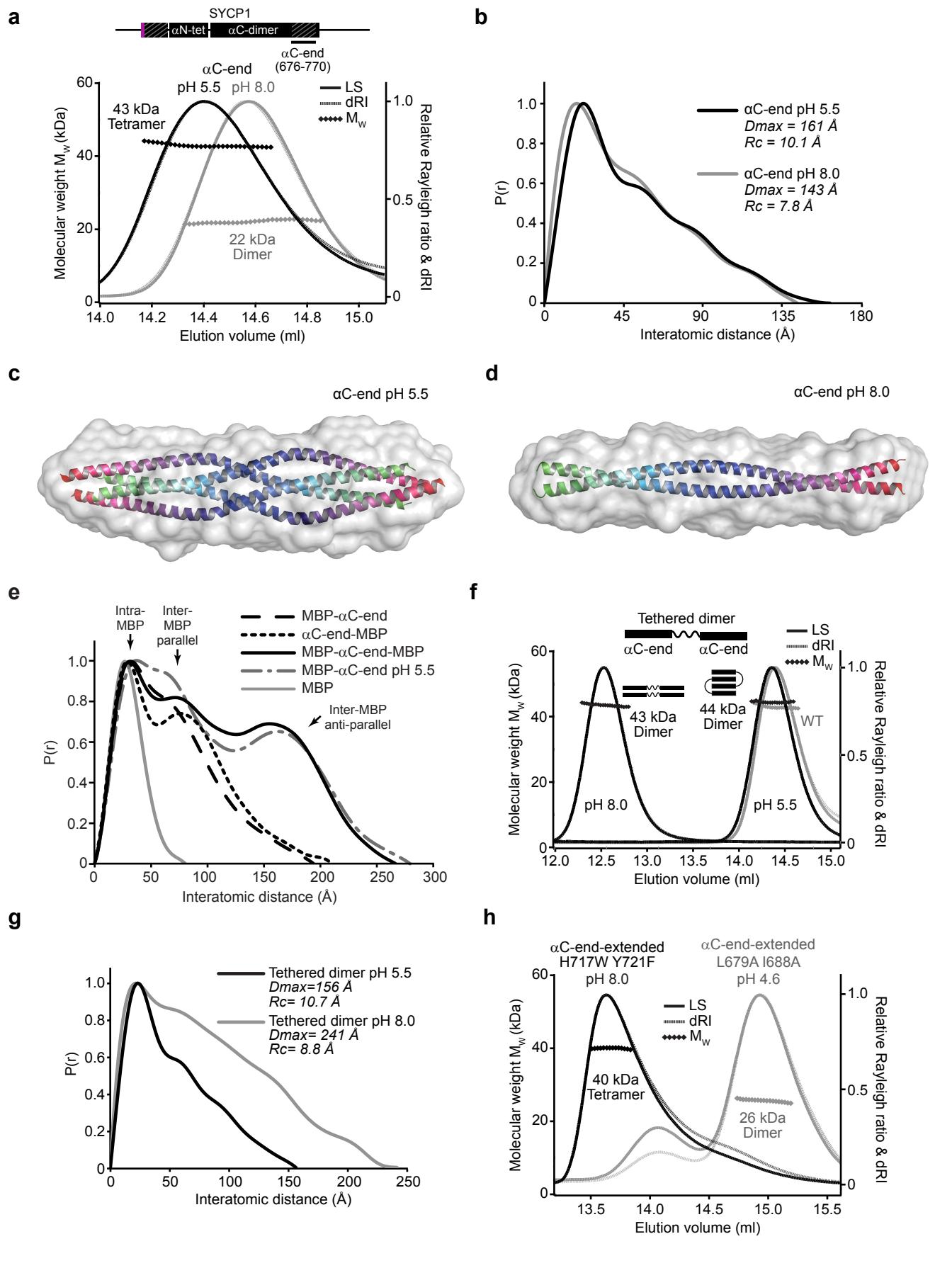
a
SYCP1
αN-tet
αC-dimer
αC-end
(676-770)
αC-end
pH 5.5
pH 8.0
LS
dRI
M_w
43 kDa
Tetramer
22 kDa
Dimer
Molecular weight M_w (kDa)
Relative Rayleigh ratio & dRI
Elution volume (ml)
b
αC-end pH 5.5
Dmax = 161 Å
Rc = 10.1 Å
αC-end pH 8.0
Dmax = 143 Å
Rc = 7.8 Å
P(r)
Interatomic distance (Å)
c
αC-end pH 5.5
d
αC-end pH 8.0
e
Intra-
MBP
Inter-
MBP
parallel
MBP-αC-end
αC-end-MBP
MBP-αC-end-MBP
MBP-αC-end pH 5.5
MBP
Inter-MBP
anti-parallel
P(r)
Interatomic distance (Å)
f
Tethered dimer
αC-end
αC-end
LS
dRI
M_w
43 kDa
Dimer
44 kDa
Dimer
WT
pH 8.0
pH 5.5
Molecular weight M_w (kDa)
Relative Rayleigh ratio & dRI
Elution volume (ml)
g
Tethered dimer pH 5.5
Dmax=156 Å
Rc= 10.7 Å
Tethered dimer pH 8.0
Dmax= 241 Å
Rc= 8.8 Å
P(r)
Interatomic distance (Å)
h
αC-end-extended
H717W Y721F
pH 8.0
αC-end-extended
L679A I688A
pH 4.6
LS
dRI
M_w
40 kDa
Tetramer
26 kDa
Dimer
Molecular weight M_w (kDa)
Relative Rayleigh ratio & dRI
Elution volume (ml)

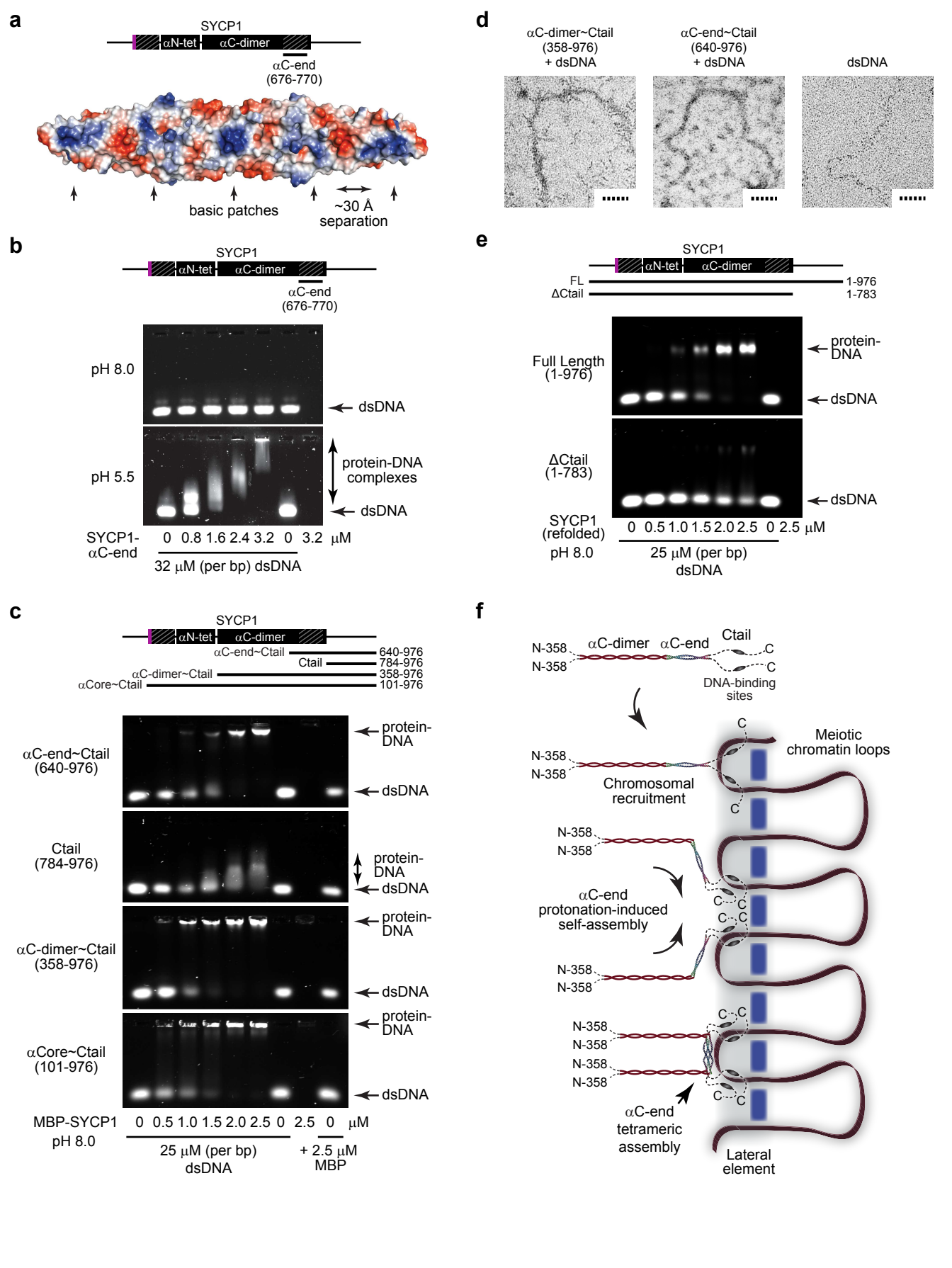
a
SYCP1
αN-tet
αC-dimer
αC-end
(676-770)
basic patches
~30 Å
separation
b
SYCP1
αN-tet
αC-dimer
αC-end
(676-770)
pH 8.0
dsDNA
pH 5.5
protein-DNA
complexes
dsDNA
SYCP1-
αC-end
0 0.8 1.6 2.4 3.2 0 3.2 μM
32 μM (per bp) dsDNA
c
SYCP1
αN-tet
αC-dimer
αC-end~Ctail
640-976
Ctail
784-976
αC-dimer~Ctail
358-976
αCore~Ctail
101-976
αC-end~Ctail
(640-976)
protein-
DNA
dsDNA
Ctail
(784-976)
protein-
DNA
dsDNA
αC-dimer~Ctail
(358-976)
protein-
DNA
dsDNA
αCore~Ctail
(101-976)
protein-
DNA
dsDNA
MBP-SYCP1
pH 8.0
0 0.5 1.0 1.5 2.0 2.5 0 2.5 0 μM
25 μM (per bp)
dsDNA
+ 2.5 μM
MBP
d
αC-dimer~Ctail
(358-976)
+ dsDNA
αC-end~Ctail
(640-976)
+ dsDNA
dsDNA
e
SYCP1
αN-tet
αC-dimer
FL
1-976
ΔCtail
1-783
Full Length
(1-976)
protein-
DNA
dsDNA
ΔCtail
(1-783)
dsDNA
SYCP1
(refolded)
pH 8.0
0 0.5 1.0 1.5 2.0 2.5 0 2.5 μM
25 μM (per bp)
dsDNA
f
N-358
αC-dimer
αC-end
Ctail
C
DNA-binding
sites
Meiotic
chromatin loops
Chromosomal
recruitment
αC-end
protonation-induced
self-assembly
αC-end
tetrameric
assembly
Lateral
element

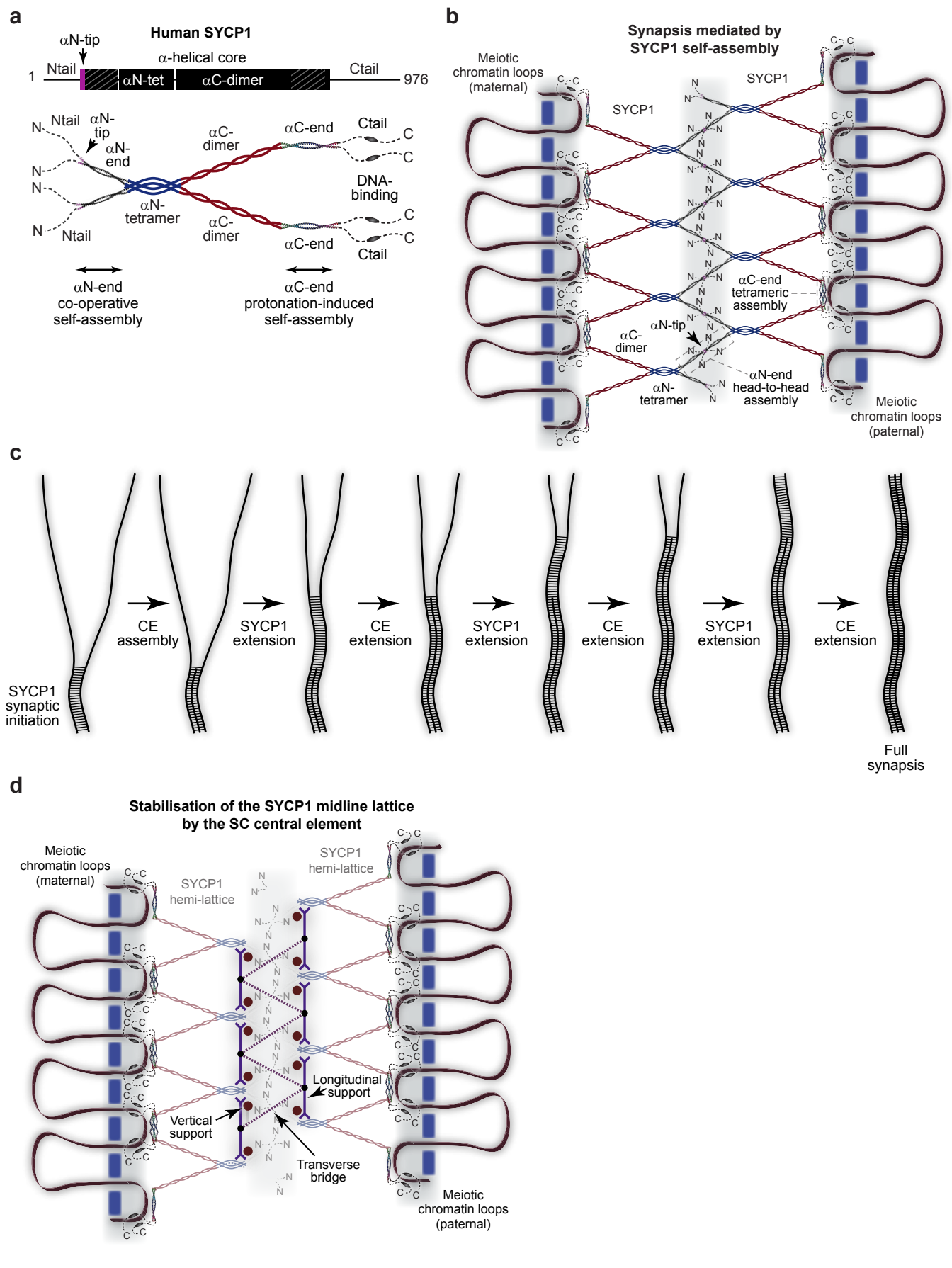
a
Human SYCP1
αN-tip
α-helical core
1
Ntail
αN-tet
αC-dimer
Ctail
976
Ntail
αN-tip
αN-end
αC-dimer
αC-end
Ctail
DNA-binding
αN-tetramer
αN-end co-operative self-assembly
αC-end protonation-induced self-assembly
b
Synapsis mediated by SYCP1 self-assembly
Meiotic chromatin loops (maternal)
SYCP1
αC-end tetrameric assembly
αN-tip
αC-dimer
αN-tetramer
αN-end head-to-head assembly
Meiotic chromatin loops (paternal)
c
SYCP1 synaptic initiation
CE assembly
SYCP1 extension
CE extension
SYCP1 extension
CE extension
SYCP1 extension
CE extension
Full synapsis
d
Stabilisation of the SYCP1 midline lattice by the SC central element
Meiotic chromatin loops (maternal)
SYCP1 hemi-lattice
SYCP1 hemi-lattice
Longitudinal support
Vertical support
Transverse bridge
Meiotic chromatin loops (paternal)